Tectonophysics 665 (2015) 127–148

Contents lists available at ScienceDirect

Tectonophysics

journal homepage: www.elsevier.com/locate/tecto

Kinematics of the Tengchong Terrane in SE Tibet from the late Eocene to early Miocene: Insights from coeval mid-crustal detachments and strike-slip shear zones

Zhiqin Xu [a,b,*], Qin Wang [b,a,*], Zhihui Cai [a], Hanwen Dong [a], Huaqi Li [a], Xijie Chen [a], Xiangdong Duan [c], Hui Cao [a], Jing Li [c], Jean-Pierre Burg [d]

[a] State Key Laboratory of Continental Tectonics and Dynamics, Institute of Geology, Chinese Academy of Geological Sciences, Beijing 100037, China
[b] State Key Laboratory for Mineral Deposits Research, Department of Earth Sciences, Nanjing University, Nanjing 210046, China
[c] Geological Survey of Yunnan Province, Kunming 650051, China
[d] Geologisches Institut, ETH Zurich, 8092 Zurich, Switzerland

ARTICLE INFO

Article history:
Received 15 July 2015
Received in revised form 25 September 2015
Accepted 28 September 2015
Available online 13 October 2015

Keywords:
Continental escape
Detachment
Strike-slip shear zone
Gneiss dome
Quartz fabrics
Tibet

ABSTRACT

It is generally believed that the extrusion of SE Tibet was bounded by the dextral Gaoligong and the sinistral Ailaoshan-Red River strike-slip shear zones from the Oligocene to early Miocene. This study integrates field mapping, structural analysis and geochronology in western Yunnan (China), where foliated Precambrian basement rocks and late Cretaceous to early Eocene plutons are exposed to the west of the Gaoligong shear zone. We found that late Eocene to early Miocene flat-lying ductile shear zones were kinematically related to steeply dipping strike-slip shear zones. Four elongated gneiss domes (Donghe, Guyong, Yingjiang and Sudian) are cored by high-grade metamorphic rocks and pre-kinematic granite plutons, and bounded by top-to-NE detachments and NE-trending dextral strike-slip shear zones. Zircon U-Pb ages from LA-ICP-MS analysis and $^{40}Ar/^{39}Ar$ ages of micas and hornblende demonstrate that the flat-lying Donghe Detachment (>35–15 Ma) and the Nabang dextral strike-slip shear zone (41–19 Ma) were sites of prolonged, mostly coeval ductile deformation from amphibolite to greenschist facies metamorphism. The Gaoligong shear zone experienced dextral shearing under similar metamorphic conditions between 32 and 10 Ma. Consistent $^{40}Ar/^{39}Ar$ ages of hornblende from the three shear zones indicate their contemporaneity at mid-crustal depth, causing the rapid exhumation and SW-ward extrusion of the Tengchong Terrane. The strain geometry and shear zone kinematics in the Tengchong Terrane are interpreted with folding of the anisotropic lithosphere around a vertical axis, i.e., the northeast corner of the Indian Plate since 41 Ma. The newly discovered NE-trending Sudian, Yingjiang, and Lianghe strike-slip shear zones are subordinate ductile faults accommodating the initially rapid clockwise rotation of the Tengchong Terrane. The detachments caused mid-crustal decoupling and faster SW-ward extrusion below the sedimentary cover, whereas the strike-slip shear zones accommodated extrusion and clockwise rotation of the Tengchong Terrane around the proto-Eastern Himalayan syntaxis since the late Eocene.

1. Introduction

The India-Eurasia collision has produced E- to SE-ward extrusion of large fragments of the Eurasian lithosphere from central Tibet towards South China and Indochina (e.g., Najman et al., 2010; Peltzer and Tapponnier, 1988; Royden et al., 2008; Tapponnier et al., 1986, 2001; Yin, 2010 and references therein). The convergence rate of the northeast corner of India towards Eurasia was 118 mm/a at ~40–45 Ma and has slowed continuously to 57 mm/a between 20 and 10 Ma (Molnar and Stock, 2009). Slowing down of the India-Eurasia convergence rate since 20 Ma coincides with the cessation of rapid Pacific trench migration and rejuvenation or initiation of tectonic activity within the Tibetan Plateau and its margins (Molnar and Stock, 2009; Royden et al., 2008; Yin, 2006, 2010). Therefore, the late Eocene–Miocene period is critical for the outward growth of the Tibetan Plateau.

The Cenozoic strike-slip shear zones in SE Tibet appear as high mountain chains along belts of medium-high grade metamorphic and mylonitic rocks, which are also sites of former suture zones and later active faulting (Burchfiel and Chen, 2012 and references therein; Metcalfe, 2006; Shen et al., 2005) (Fig. 1). These strike-slip

* Corresponding authors at: State Key Laboratory of Continental Tectonics and Dynamics, Institute of Geology, Chinese Academy of Geological Sciences, Beijing 100037, China. Tel.: +86 10 6832 9504; fax: +86 10 6899 9663.
E-mail addresses: 3077864156@qq.com (Z. Xu), qwang@nju.edu.cn (Q. Wang).

http://dx.doi.org/10.1016/j.tecto.2015.09.033

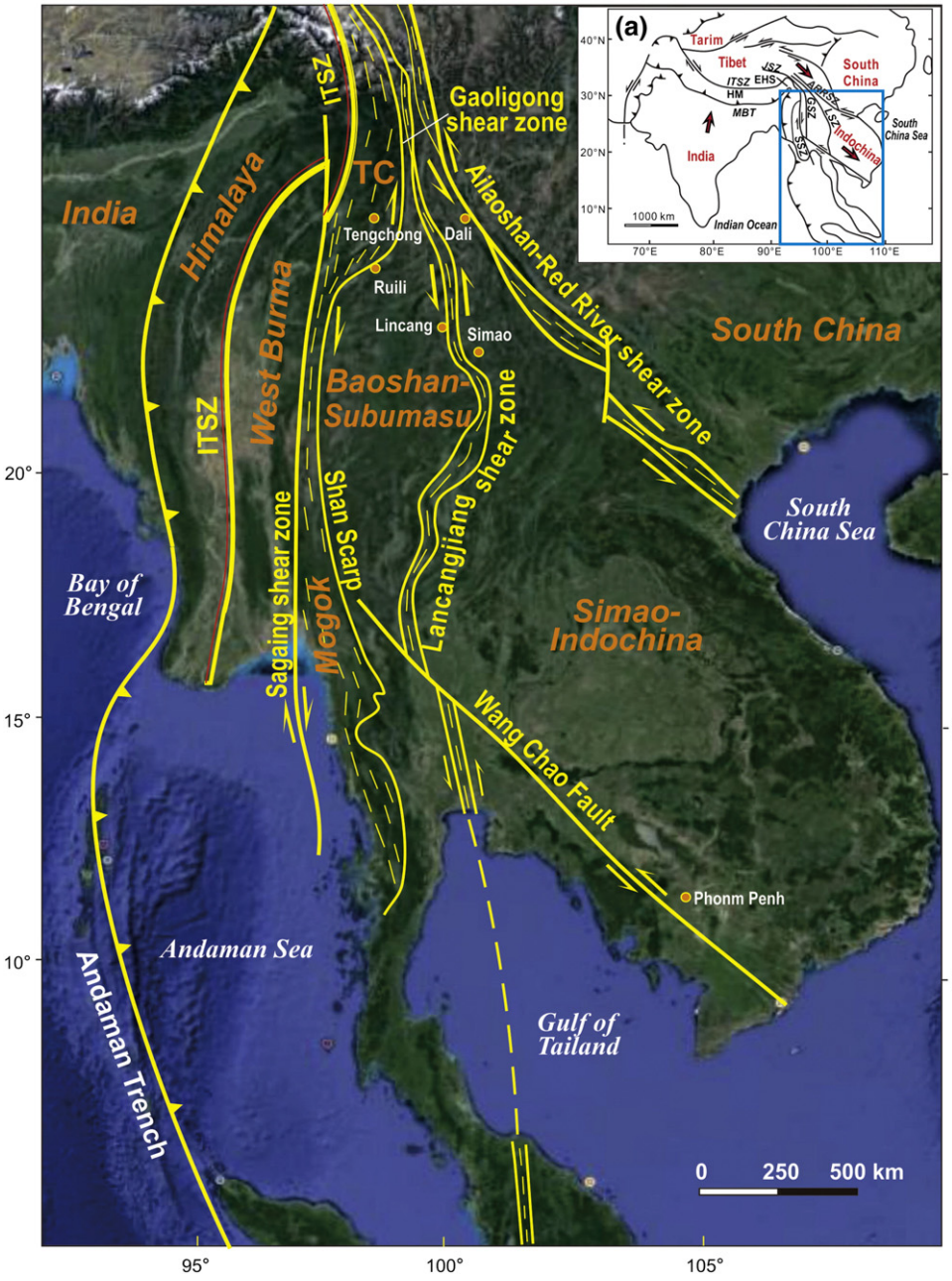

Fig. 1. Topography and schematic tectonic map of SE Tibet and adjacent regions. Bold yellow lines are major faults or ductile shear zone in the early Miocene, double lines show the Indus-Tsangpo Suture Zone (ITSZ), and dashed yellow thin lines indicate the dominant trend of stretching lineation in ductile shear zones. Red arrows in the inset map indicate motion of India, Indochina and eastern Tibet relative to Siberia from GPS observations (Shen et al., 2005; Zhang et al., 2004). The extrusion of SE Asia is bounded by the sinistral strike-slip Ailaoshan-Red River shear zone (ARRSZ) in the northeast and the dextral strike-slip Sagaing fault in the west (Tapponnier et al., 2001). Abbreviations: GSZ, Gaoligong shear zone; LSZ, Lancangjiang shear zone; EHS, eastern Himalayan syntaxis; HM, Himalayan orogen; MBT, main boundary thrust; TC, Tengchong Terrane.

shear zones have accommodated large displacements related to the southeastward extrusion of continental fragments during the India-Eurasia collision.

The 'tectonic escape' model attributes lateral extrusion of SE Tibet to block motion along subvertical lithospheric fault zones such as the dextral Gaoligong and the sinistral Ailaoshan-Red River strike-slip shear zones (Leloup et al., 2001; Tapponnier and Molnar, 1976; Tapponnier et al., 1986). In contrast, England and Houseman (1986) proposed that the continental lithosphere of the Tibetan Plateau behaves as a 'thin viscous sheet', which deformed first by diffuse crustal thickening and then by strike-slip faulting in the shallow crust. The 'crustal flow' model puts forward that the lower crust material of the Tibetan Plateau has been enough thermally weakened to flow outwards within a vertically decoupled lithosphere (Clark and Royden, 2000; Royden et al., 2008). Although these end-member models have been widely used to interpret the lateral expansion of the Tibetan Plateau, the present-day velocity field from GPS measurements consists of both a rigid rotational component and an internal strain component, which calls for new models to fit different regions (e.g., Gan et al., 2007; Shen et al., 2005; Thatcher, 2007; Zhang et al., 2004).

Subhorizontal shear zones have been recognized in a few exposed metamorphic basement areas in SE Tibet, such as along the Red River shear zone in north Vietnam (Jolivet et al., 2001), in the Mogok metamorphic belt in Burma (Bertrand et al., 1999, 2001; Searle et al., 2007), and in the Ruili and Diancangshan metamorphic belts in western Yunnan province (China) (Liu et al., 2007; Socquet and Pubellier, 2005). Although subhorizontal fabrics in high-grade metamorphic rocks could be evidence of deep crustal flow (e.g., Beaumont et al., 2001;

Bonamici et al., 2011; Dumond et al., 2010), they may also represent low-angle detachments or flat-ramp basal thrusts during formation of gneiss domes (Yin, 2004). Because of complex inherited structures and multi-magmatism from the Paleozoic to early Cenozoic, the temporal and spatial relationships between the flat-lying and strike-slip shear zones in SE Tibet remain poorly understood. How the kinematic displacement of the shear zones accommodated the discrepancy between paleomagnetic and GPS-determined tectonic rotation around the eastern Himalayan syntaxis (Kornfeld et al., 2014a; Otofuji et al., 2010) has not been investigated.

The Tengchong Terrane in SE Tibet lies between the Indus-Tsangpo Suture Zone (ITSZ) and the Gaoligong strike-slip shear zone (Fig. 1). It is a key area to trace the transition from a compressional regime in the Himalayas to clockwise rotation around the eastern Himalayan syntaxis. We present an integrated study of mapping, structural analysis and geochronology in the Tengchong Terrane. We found that NNE-trending strike-slip shear zones were activated at the same time as top-to-NE detachments in late Eocene to early Miocene period. The strike-slip shear zones controlled the rotation of the Tengchong Terrane and formed the arcuate structures, whereas the subhorizontal detachments accommodated exhumation of high-grade metamorphic rocks and Cretaceous to early Eocene granite plutons. The reconstructed structural framework of the Tengchong Terrane reveals a fault-related gneiss dome system during tectonic extrusion of SE Tibet.

2. Geological setting

The SE Tibetan Plateau is bounded by the ITSZ to the west and the Ailaoshan-Red River shear zone (ARRSZ) to the east (Fig. 1). The nearly N-S striking Gaoligong and Lancangjiang strike-slip shear zones divide the SE Tibetan Plateau into, from west to east, the Tengchong-West Burma-Mogok Block, the Baoshang-Subumasu Block and the Simao-Indochina Block (e.g., Akciz et al., 2008; Armijo et al., 1989; Burchfiel and Chen, 2012; Bureau of Geology and Mineral Resources of Yunnan Province, 1990; Harrison et al., 1996; Searle et al., 2007; Wang and Burchfiel, 1997; Zhang et al., 2012). The N-S striking dextral Sagaing shear zone offsets the ITSZ by ~100 km and separates the Tengchong Terrane and the Mogok metamorphic belt from the West Burma Terrane (Ratschbacher et al., 1996; Wang et al., 1998).

The Tengchong Terrane between the ITSZ and the Gaoligong strike-slip shear zone (Fig. 2) contains high-grade metamorphic rocks, Devonian-Permian sedimentary rocks, Mesozoic-Cenozoic granites, early Pliocene to Holocene volcanic rocks (Kornfield et al., 2014b; Li et al., 2000) and small Neogene basins (Burchfiel and Chen, 2012 and references therein; Bureau of Geology and Mineral Resources of Yunnan Province, 1990; Wang and Burchfiel, 1997). The high-grade metamorphic rocks are traditionally regarded as the Precambrian basement of the Tengchong Terrane and attributed to the Gaoligong Group (Bureau of Geology and Mineral Resources of Yunnan Province, 1990), which extends southward to join with the Mogok metamorphic belt

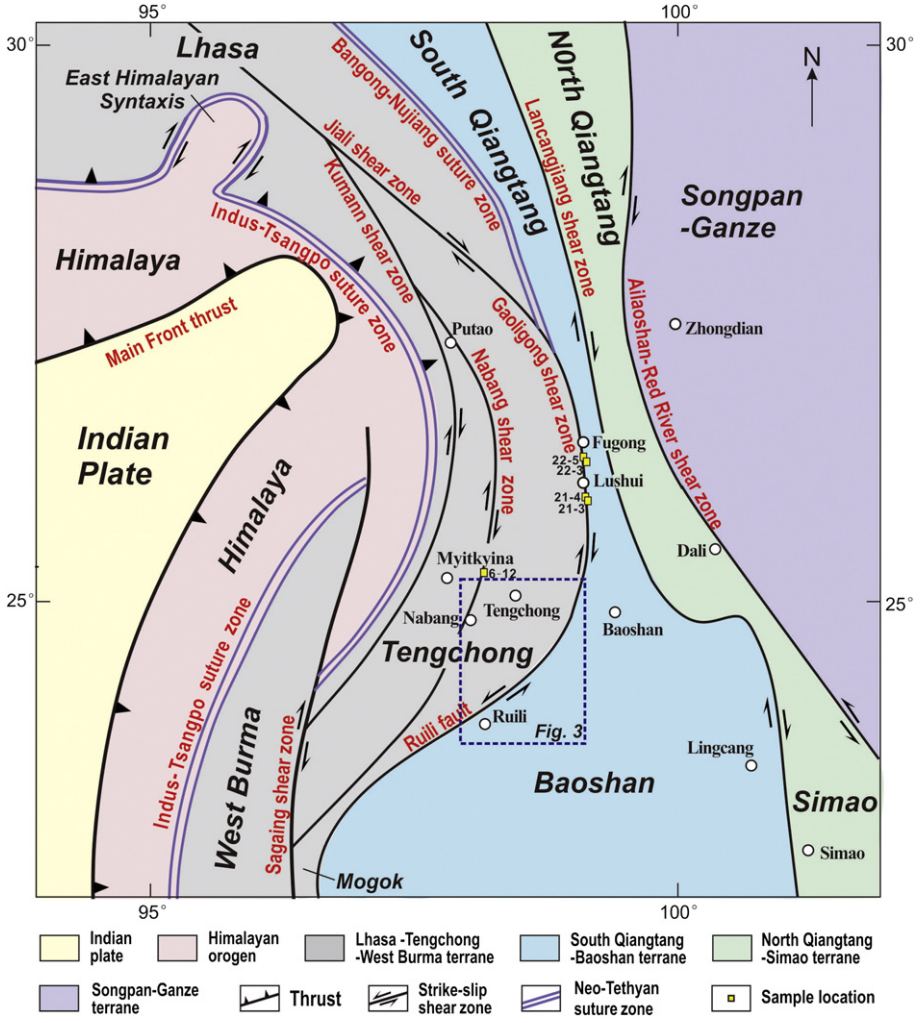

Fig. 2. Simplified tectonic framework of the Tengchong Terrane and adjacent regions. The study area is marked by the blue rectangle in dashed lines. Double purple lines and bold black lines illustrate the suture zones, and major faults or ductile shear zone, respectively.

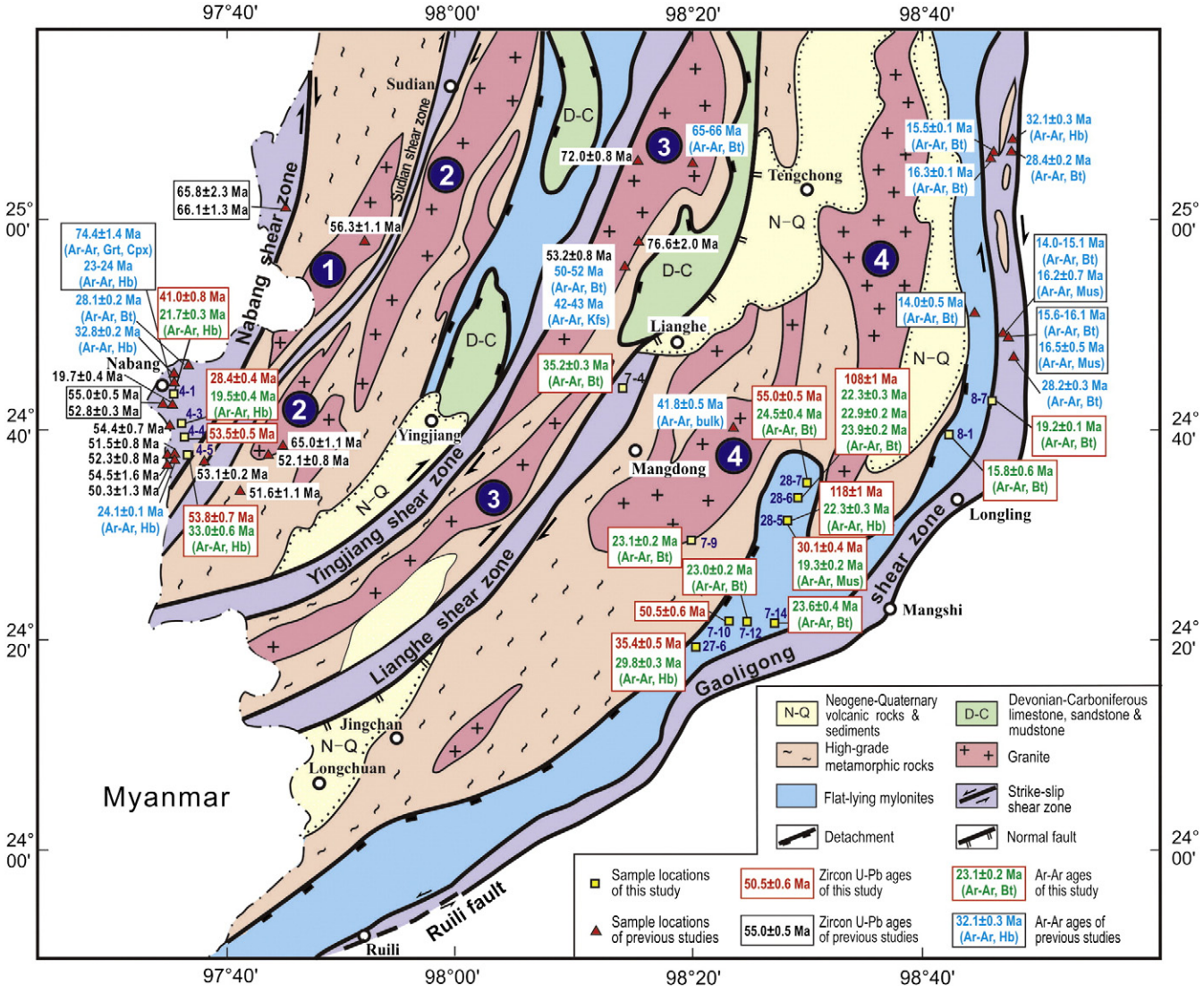

Fig. 3. Simplified geological map of the Tengchong Terrane in western Yunnan province (modified after the unpublished 1: 250,000 Geological Map of Luxi County, *Geological Survey of Yunnan Province*, 2008) with geochronological data. White numbers in circles indicate granite plutons in this region: 1. Sudian pluton; 2. Yingjiang pluton; 3. Guyong pluton; 4. Donghe pluton. U-Pb zircon ages from previous studies (Ma et al., 2013; Qi et al., 2015; Xu et al., 2012; Yang et al., 2009) and this study are shown in black and red, respectively. $^{39}Ar/^{40}Ar$ ages of biotite (Bt), muscovite (Mus), hornblende (Hb), K-feldspar (Kfs), garnet (Grt) and clinopyroxene (Cpx), as well as $^{39}Ar/^{40}Ar$ ages of bulk mafic dykes (bulk) are also given in blue for previous studies (Dong et al., 2006; Ji et al., 2000; Lin et al., 2009; Wang et al., 2006; Xu et al., 2009; Zhang et al., 2012) and in green for this study. Sample locations of this study are labelled by the first two numbers in a sample number.

(Mitchell, 1993). $^{40}Ar/^{39}Ar$ mica ages yield cooling of the Mogok metamorphic belt at 21–17 Ma (Bertrand et al., 1999, 2001).

The Gaoligong Group records early Paleozoic (547–454 Ma) pervasive anatexis with few granitic intrusions (Cai et al., 2013; Lin et al., 2012). Mesozoic-Cenozoic deformation was accompanied by three magmatic episodes: (1) early Cretaceous (126–108 Ma) in the eastern Tengchong Terrane, (2) late Cretaceous (76–66 Ma) in the central and western Tengchong Terrane, and (3) Paleocene to early Eocene (66–50 Ma) in the western and eastern Tengchong Terrane (Ma et al., 2013, 2014; Qi et al., 2015; Xu et al., 2012; Yang et al., 2009; Zhu et al., 2015). These granitoids are comparable to the 120–55 Ma granitoids of the Gangdese batholith in southern Tibet (Zhu et al., 2011). Similar early Cretaceous to Oligocene plutons and dykes have also been reported in the Mogok metamorphic belt (Mitchell et al., 2012; Searle et al., 2007). Therefore, the Gangdese magmatic arc, the Tengchong Terrane, and the Mogok metamorphic belt have been structurally linked since the early Cretaceous.

3. Gneiss domes in the Tengchong Terrane

A gneiss dome is composed of a metamorphic-plutonic complex in the core and high-grade schists and gneisses around, and overlain by supracrustal strata (Eskola, 1949). Plutonic rocks make up nearly one third of the Tengchong Terrane. Zircon U-Pb ages provide crystallization

Fig. 4. (a) Simplified geological map of the Tengchong Terrane in western Yunnan province with sample locations and attitudes of foliation (modified after the unpublished 1: 250,000 Geological Map of Luxi County, *Geological Survey of Yunnan Province*, 2008). Lower hemisphere projection of the foliation and stretching lineation of the Donghe Detachment is from (b) the northern Longling area, (c) the western Mangshi area, and (d) the northern Ruili area (labeled as b, c, d in the geological map). (e) NW-trending cross-section AA′ and (f) NE-trending cross-section BB′ in the southern Tengchong Terrane. White numbers indicate granite plutons in this region: 1. Sudian pluton; 2. Yingjiang pluton; 3. Guyong pluton; 4. Donghe pluton. Sample locations are labelled by the first two numbers in a sample number.

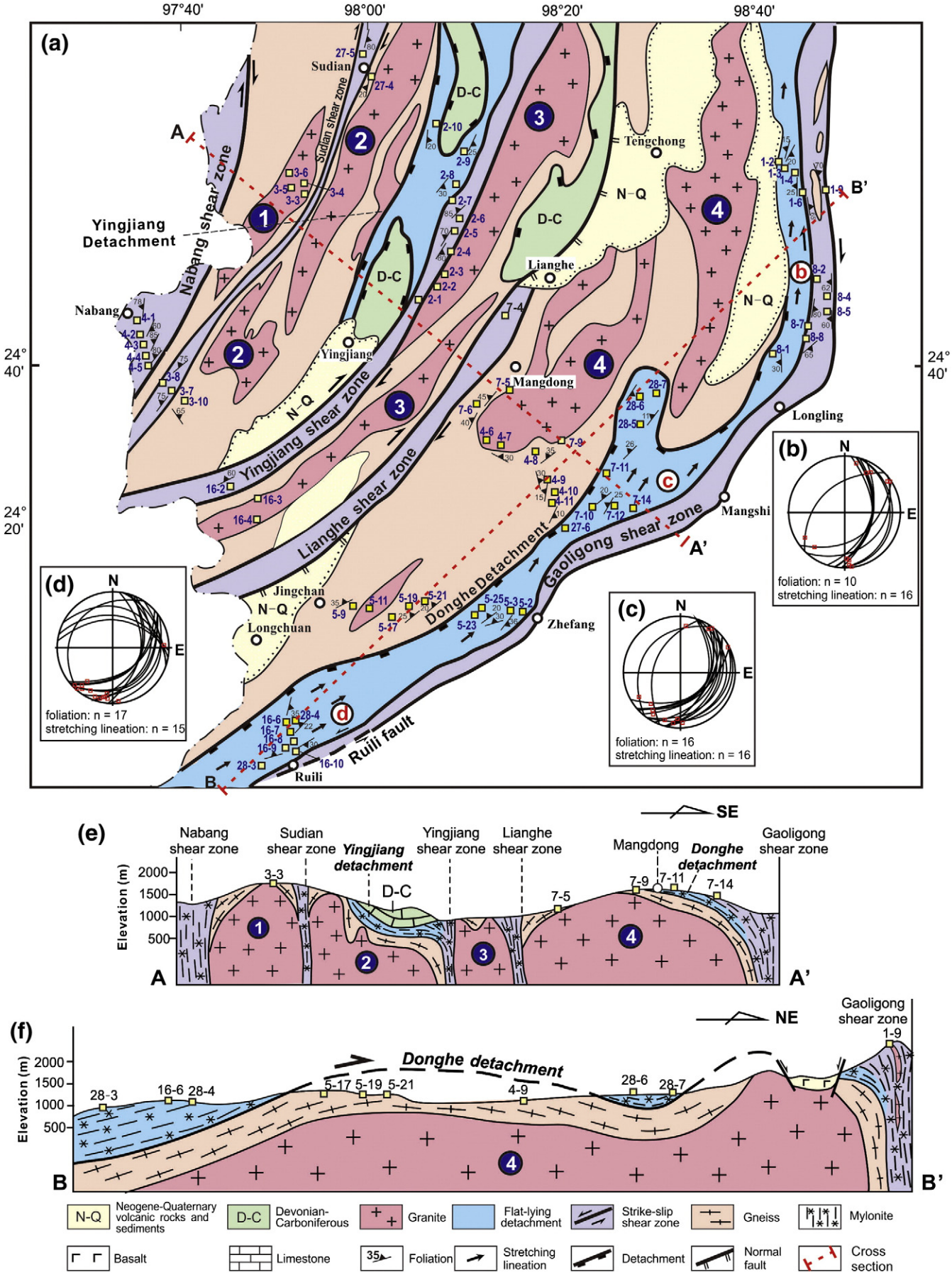
(a)
97°40'
98°00'
98°20'
98°40'
24° 40'
24° 20'
Sudian
Tengchong
Lianghe
Nabang
Yingjiang
Mangdong
Longling
Mangshi
Jingchan
Longchuan
Zhefang
Ruili
Yingjiang Detachment
Nabang shear zone
Sudian shear zone
Yingjiang shear zone
Lianghe shear zone
Donghe Detachment
Gaoligong shear zone
Ruili fault
N-Q
D-C
A
A'
B
B'
(b)
foliation: n = 10
stretching lineation: n = 16
(c)
foliation: n = 16
stretching lineation: n = 16
(d)
foliation: n = 17
stretching lineation: n = 15
(e)
SE
Nabang shear zone
Sudian shear zone
Yingjiang detachment
Yingjiang shear zone
Lianghe shear zone
Mangdong
Donghe detachment
Gaoligong shear zone
Elevation (m)
2000
1500
1000
500
(f)
NE
Gaoligong shear zone
Donghe detachment
Elevation (m)
N-Q Neogene-Quaternary volcanic rocks and sediments
D-C Devonian-Carboniferous
Granite
Flat-lying detachment
Strike-slip shear zone
Gneiss
Mylonite
Basalt
Limestone
Foliation
Stretching lineation
Detachment
Normal fault
Cross section

ages of the Sudian pluton (~56 Ma), the Yingjiang pluton (65–52 Ma), the Guyong pluton (76–53 Ma), and the Donghe pluton (127–118 Ma) (Ma et al., 2013; Qi et al., 2015; Xu et al., 2012; Yang et al., 2009) (Fig. 3). $^{40}Ar/^{39}Ar$ dating of biotite from these granites yields two cooling stages at 68–65 Ma and at 52–50 Ma, close to zircon U-Pb ages and Rb-Sr isochronal ages of the same rocks (Dong et al., 2006; Jiang et al., 2012) (Fig. 3). This suggests that the late Cretaceous to early Eocene granites quickly cooled down to ~300 °C after intrusion.

Metamorphic and foliated rocks around these granite plutons were generally mapped as the Gaoligong Group (Bureau of Geology and Mineral Resources of Yunnan Province, 1990). However, new geochronological data demonstrate that the high-grade metamorphic rocks also contain granitoids strongly deformed during the early Cretaceous and the Oligocene (Fig. 3). We first focus on the structural relationships between the granites and the elongated domal structures shaped by regional foliation.

To the west of the Gaoligong strike-slip shear zone, new mapping identified widespread mylonitic ortho- and paragneisses with gently dipping foliation and nearly horizontal stretching lineation defined by long axes of amphibole and sillimanite grains and boudinage of felsic veins (Fig. 4a). Despite the varying attitude of the foliation, the stretching lineation has a consistent NE-azimuth, parallel to the strike of the Gaoligong shear zone. These strongly sheared rocks can be traced for more than 100 km from the northern Longling area (Fig. 4b), the western Mangshi area (Fig. 4c), to the northern Ruili area (Fig. 4d), forming a gently folded, low-angle ductile shear zone around the Donghe pluton. We name this shear zone the Donghe Detachment.

The subhorizontal fabrics in high-grade metamorphic rocks surrounding the Donghe pluton (Figs. 5a–c) are consistent with the overlying mylonites of the Donghe Detachment (Fig. 5d). Numerous felsic veins intrude into the high-grade metamorphic gneisses and mylonites and show boudinage where parallel to the foliation (Figs. 5c–d), suggesting that they are syn-kinematic veins to the Donghe Detachment. In addition, no matter the lineation plunges SW or NE, a top-to-NE or a top-to-the-north shear sense is everywhere documented by drag folds, S-C fabrics, micafishes, and σ- and δ-type feldspar porphyroclasts (Fig. 6). The Donghe gneiss dome is thus cored by high-grade metamorphic rocks and early Cretaceous granites, and topped by the Donghe Detachment.

The structural relationship between the Donghe pluton and the Donghe Detachment is well exposed in the northwestern Mangshi area, where a 1 km-thick foliated granite sheet lies within flat-lying mylonites of the Donghe Detachment (site 28–5 in Fig. 4). The granite sheet is characterized by a gently dipping magmatic fabric, numerous enclaves and felsic veins. The core of this granitic sheet is weakly deformed (Fig. 5f), whereas strain assessed from foliation intensity/spacing increases outward to the sheet edges. Accordingly, ductile shear due to the Donghe Detachment started with or after intrusion of this granite sheet. The foliation of this granite sheet and surrounding mylonites changes gradually eastward from sub-horizontal to nearly

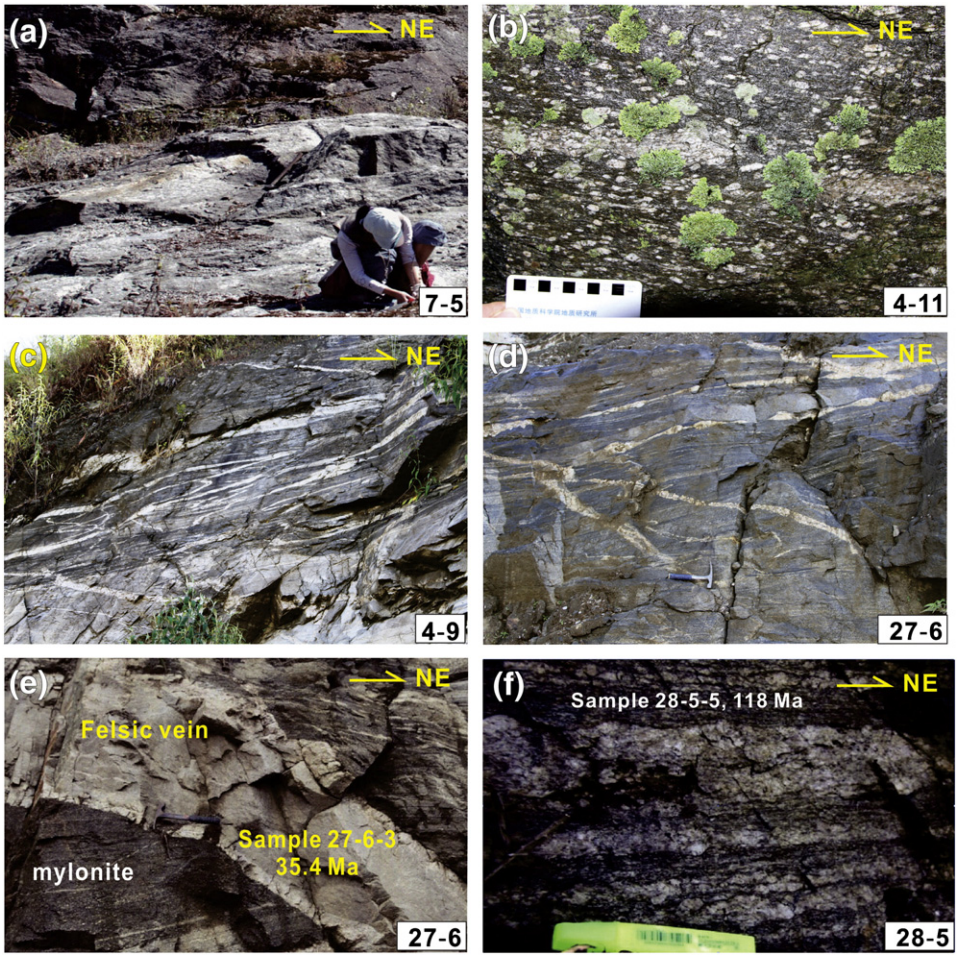

Fig. 5. Outcrop observations in the Donghe gneiss dome. (a) A flat lying foliation in granitic gneiss next to the Donghe pluton (site 7-5 in south Mangdong). (b) Augen gneiss with a penetrative flat foliation and top-to-NE shear sense (site 4-11 in east Mangdong). (c) Flat lying granitic gneiss with folded, parallel veins and oblique, undeformed veins (site 4-9 in east Mangdong). (d) Flat lying felsic mylonite intruded by boudinaged parallel felsic veins, and (e) an undeformed felsic vein with chilled contacts against mylonite (site 27-6 in east Mangdong). (f) Foliated granite with magmatic fabrics (site 28-5 in east Mangdong).

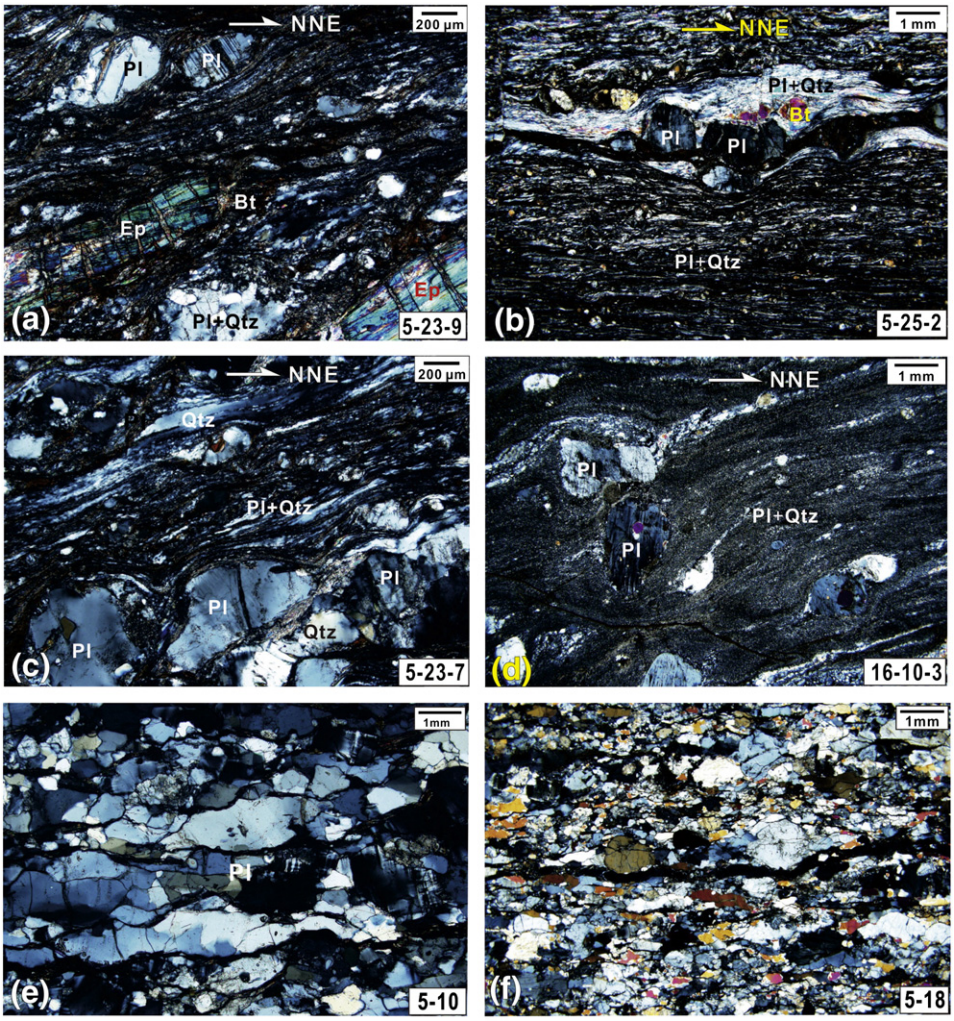

Fig. 6. Microstructures of mylonites and mylonitic gneisses from the Donghe gneiss dome, showing a top-to-the-NNE shear sense. (a) σ-type plagioclase porphyroclasts in epidote-bearing mylonitic paragneiss, (b) shear bands composed of recrystallized plagioclase and quartz in felsic mylonite, (c) core-mantle structure of plagioclase and quartz ribbons in felsic mylonite, (d) σ-type plagioclase porphyroclasts in felsic ultramylonite, and (e–f) foliation defined by recrystallized quartz in granitic gneiss. Thin sections are perpendicular to the foliation and parallel to the stretching lineation (XZ thin section), crossed polarized light. Abbreviations: Bt, biotite; Ep, epidote; Pl, plagioclase; Qtz, quartz.

vertical next to the Gaoligong strike-slip shear zone (Fig. 4e), implying coeval activation of the steeply dipping Gaoligong shear zone and the flat-lying detachment.

A similar sub-horizontal ductile shear zone, the Yingjiang Detachment, is found between the Paleocene Yingjiang granite pluton and the overlying Devonian-Carboniferous sedimentary sequence (Fig. 4). The Yingjiang Detachment contains mylonitic schists and phyllites that were intruded by foliation-parallel felsic veins. It is also characterized by the nearly N-S-trending stretching lineation and top-to-the-north shear sense. The denudation of the Yingjiang gneiss dome is less significant than for the Donghe gneiss dome because the Paleozoic sedimentary cover is still preserved.

The Guyong and Sudian plutons are also surrounded by foliated high-grade metamorphic rocks with subhorizontal foliation, NE-trending stretching lineation, and top-to-NE shear sense. However, we did not find mylonites above these metamorphic rocks, likely because both the overlying detachment and Paleozoic sediments have been eroded. We propose that the Tengchong Terrane is a gneiss dome system composed of the NE-trending, elongated Donghe, Guyong, Yingjiang, and Sudian gneiss domes (Fig. 4). Fig. 7 presents the lithological column of this terrane with seven units from top to bottom: (1) Pliocene to Quaternary volcanic rocks; (2) Devonian-Carboniferous sedimentary cover, (3) mylonitic schist/phyllite, (4) mylonitic sillimanite-bearing paragneiss, (5) granitic mylonite and mylonitic granite, (6) granite with magmatic fabrics, and (7) Cretaceous to Eocene porphyritic granite and medium to fine-grained granite. Because the shear sense on a low-angle shear zone is a relative motion, a huge amount of lithospheric materials beneath the detachments has moved southwestward.

4. Strike-slip shear zones in the Tengchong Terrane

4.1. The Gaoligong shear zone

As the boundary between the Tengchong and Baoshan Terranes, the nearly N-S trending Gaoligong strike-slip shear zone is regarded as the southern continuation of the Bangong-Nujiang Suture Zone, which separates the Lhasa Terrane from the South Qiangtang Terrane (Fig. 2). To the south, the Gaoligong shear zone strikes NE and joins with the Shan scarp (e.g., Burchfiel and Chen, 2012; Bureau of Geology and Mineral Resources of Yunnan Province, 1990; Wang and Burchfiel, 1997; Wang et al., 2006, 2008). The Jiali strike-slip shear zone was initiated as a sinistral shear zone in the early Miocene, then changed to dextral motion and linked with the Gaoligong shear zone since ~18 Ma (Lee et al., 2003). Previous studies obtained hornblende $^{40}Ar/^{39}Ar$ ages of ~32 Ma along

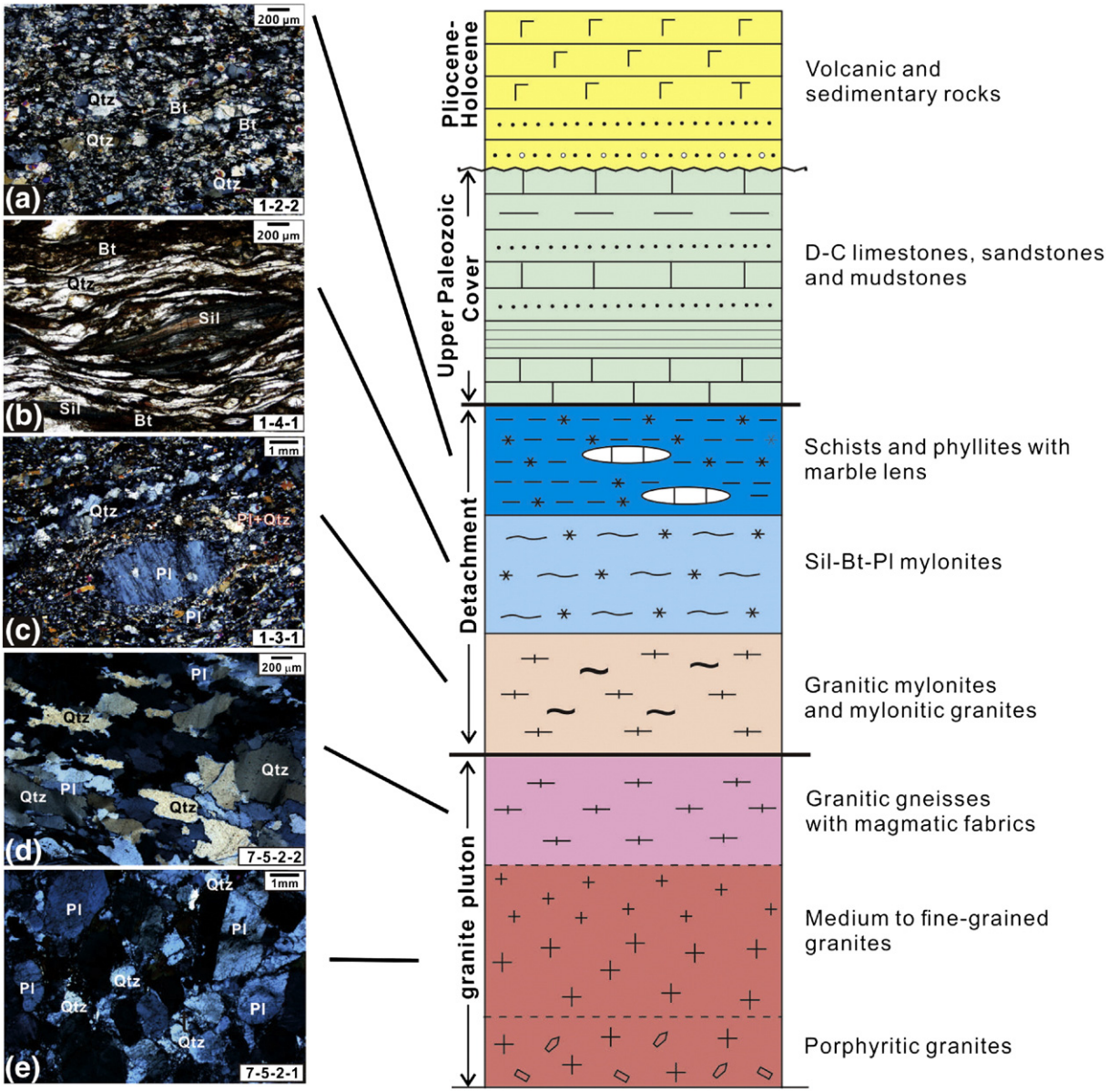

Fig. 7. A lithological column of the Tengchong Terrane with typical samples from the Donghe gneiss dome. XZ thin section, crossed polarized light. Abbreviations: Bt, biotite; Pl, plagioclase; Qtz, quartz; Sil, sillimanite.

the Gaoligong shear zone, whereas $^{40}Ar/^{39}Ar$ ages of biotite and muscovite suggest the main foliation in the Gaoligong and Jiali shear zones at 18–10 Ma and 22–11 Ma, respectively (Fig. 3) (Lee et al., 2003; Lin et al., 2009; Wang et al., 2006; Zhang et al., 2012). To the south, the Gaoligong shear zone was overprinted by the NE-striking sinistral Ruili fault. Fission-track data indicate that the footwall of the Ruili fault (i.e., the Gaoligong shear zone) experienced fast cooling between 8.4 and 0.9 Ma, because of normal faulting along boundaries of the Gaoligong shear zone (Wang et al., 2008).

Field observations along the Gaoligong Mountains (Fig. 4) confirmed that the 500-m to 6-km wide Gaoligong shear zone contains mylonitic granitic gneisses, paragneisses, quartz schists and marble lens, and is characterized by steep foliation and nearly N-S trending subhorizontal stretching lineation (Fig. 8a). The banded mylonitic rocks were tightly folded with the hinges parallel to the lineation (Fig. 8b). S-C fabrics in shear bands (Fig. 8c) and asymmetric boudins of quartz veins (Figs. 8d) at outcrops indicate dextral movement, in agreement with σ-type plagioclase porphyroclasts (Figs. 8e–f), S-C fabric (Fig. 8g) and shear-band type fragmented biotite porphyroclasts (Fig. 8h) in thin sections. Subgrain rotation recrystallization and grain boundary migration are dominant in quartz (Figs. 8e–h), suggesting deformation under medium temperature (400–500 °C) (Passchier and Trouw, 2005).

4.2. The Nabang shear zone

Zhong (1998) first described the NE-striking Nabang shear zone as a dextral strike-slip shear zone, which was subjected to granulite facies metamorphism at 76–74 Ma and amphibolite facies metamorphism at 24–23 Ma (Ji et al., 2000). Due to similar structural features and coeval shearing with the Gaoligong strike-slip shear zone, Wang et al. (2006) regarded the Nabang shear zone as a branch of the Gaoligong shear zone system. Ma et al. (2014) dated gneissic granites, mylonites and

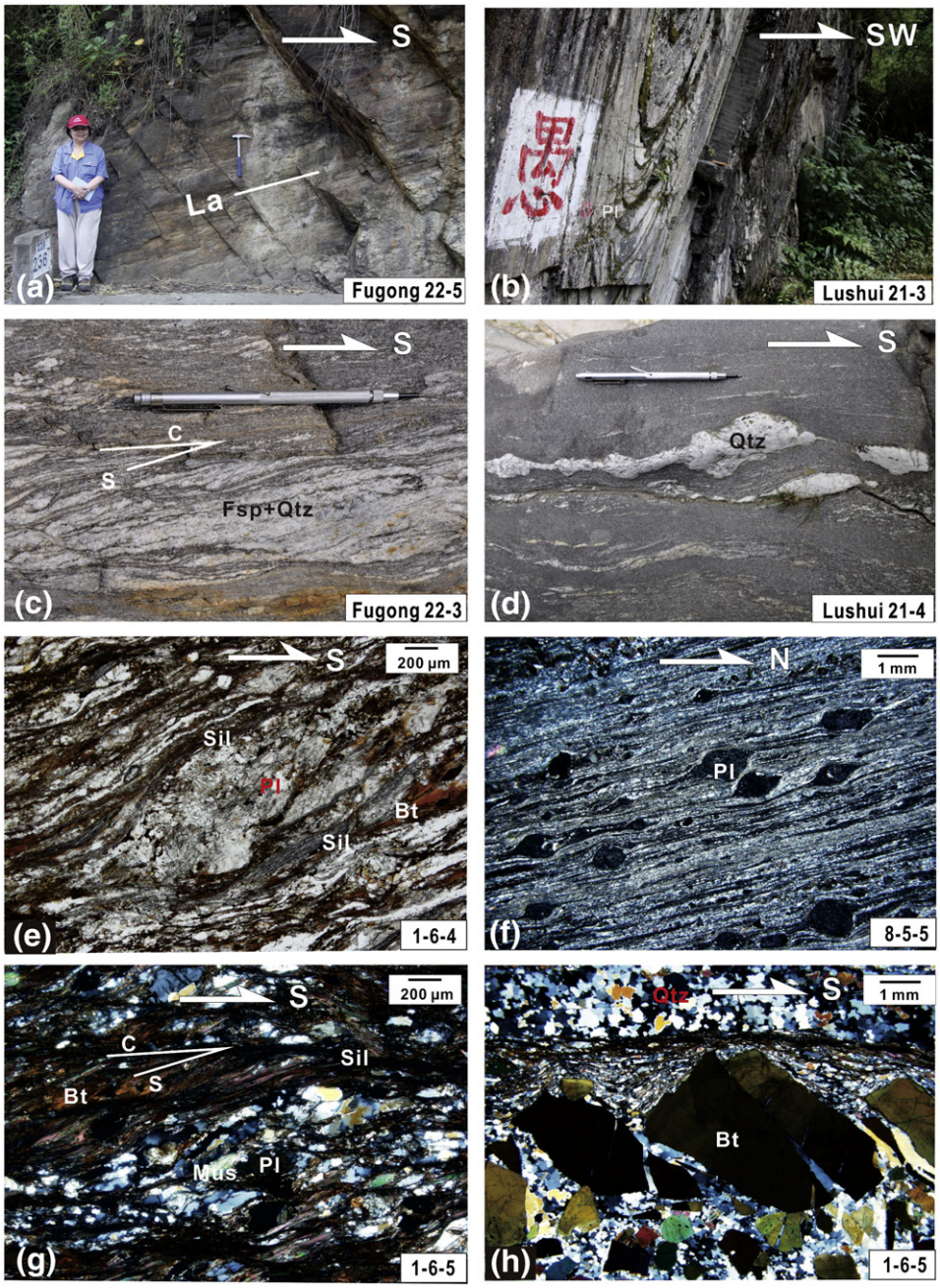

Fig. 8. Outcrop observations and microstructures of the Gaoligong strike-slip shear zone. (a) Subhorizontal N-plunging lineation in steeply dipping mylonitic gneiss (site 22-5 in Fugong area). (b) Folded schist with the N-trending hinges parallel to the stretching lineation (site 21-3 in Lushui area). (c) S-C fabric in shear bands of migmatite (site 22-3 in Fugong area) and (d) asymmetric boundins of quartz veins in felsic mylonite (site 21-4 in Lushui area). Dextral shear sense can be determined from σ-type plagioclase porphyroclasts in (e) sillimanite-biotite-plagioclase mylonite and (f) phyllite, (g) S-C fabric and (h) fragmented biotite porphyroclasts in sillimanite-bearing mylonite. XZ thin sections. Panel (e) is under plane polarized light, and panels (f-h) are under crossed polarized light. Mineral abbreviations: Bt, biotite; Pl, plagioclase; Qtz, quartz; Mus, muscovite; Sil, sillimanite. Sample locations are given in Fig. 2 and Fig. 4.

migmatites in the Nabang area and found that the metamorphosed granitoids crystallized in the early Eocene (~50–55 Ma) (Fig. 3).

Field work in Nabang and eastern Myitkyina area delimited the 3–4 km wide Nabang shear zone in which mylonites, garnet-sillimanite paragneisses and amphibole-feldspar gneisses developed a steeply dipping foliation with N-S trending and sub-horizontal stretching lineation (Figs. 9a–b). Granitic sheets vary from concordant to weakly discordant with respect to the foliation in high strain zones, indicating partial melting during shearing (Fig. 9b). Dextral shearing is documented by asymmetric fabrics at outcrops (Figs. 9c–d) and in thin sections (Figs. 9e–h). Deformation occurred at 500–600 °C according to the core-mantle structure of feldspar (Figs. 9e–f), lobate grain boundaries quartz and plagioclase (Figs. 9f–g), and myrmekite growth along the boundaries of K-feldspar porphyroclasts (Fig. 9g).

4.3. The Sudian, Yingjiang and Lianghe shear zones

In this study, we recognized three NNE- to NE-trending dextral strike-slip shear zones in the southern Tengchong Terrane, and refer to them, from west to east, as the Sudian, Yingjiang, and Lianghe shear zones (Fig. 4).

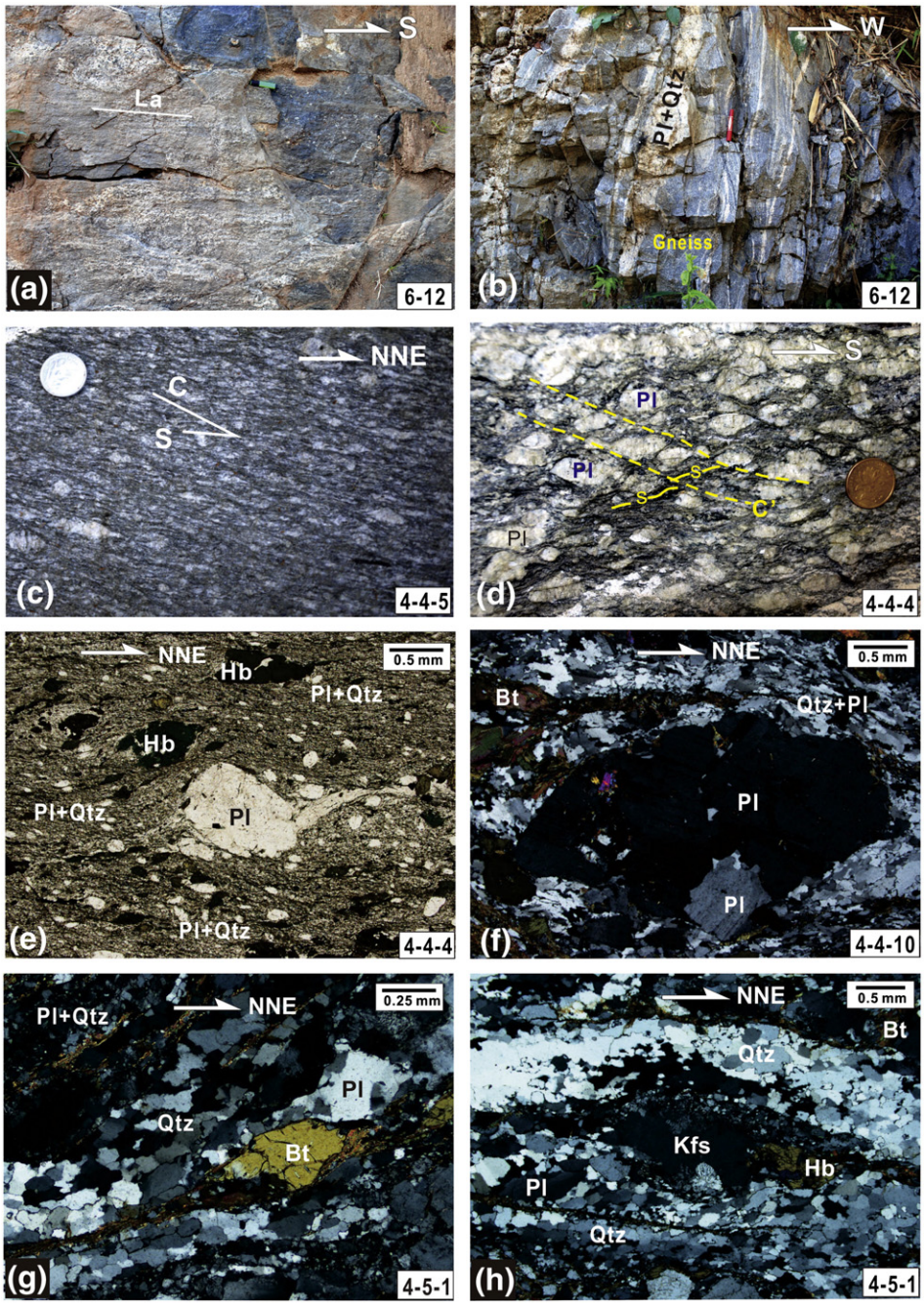

Fig. 9. Outcrop observations and microstructures of the Nabang strike-slip shear zone. (a) Subhorizontal lineation in steeply dipping mylonitic gneiss, and (b) banded gneiss with concordant granite sheets parallel to foliation (site 6-12 near Myitkynia). (c) S-C fabric and (d) S-C′ fabric from granitic mylonites (site 4-4 near Nabang village) illustrate a dextral shear sense. XZ thin sections from granitic mylonites near Nabang village show (e) δ-type and (f) σ-type plagioclase porphyroclasts, (g) mica fish, and (h) myrmekite along grain boundaries of K-feldspar. Sample location of site 6-12 is given in Fig. 2, while other sample locations are shown in Fig. 4.

The Sudian strike-slip shear zone is ~500–700 m wide and comprises mylonitic sillimanite-biotite-garnet paragneisses and orthogneisses. It separates the Sudian and Yingjiang gneiss domes and is characterized by steep NWW-dipping foliation, sub-horizontal stretching lineation and dextral shear sense (Figs. 10a-b).

The Guyong dome is bounded by the NE-striking Yingjiang strike-slip shear zone in the west, and the Lianghe strike-slip shear zone in the east (Fig. 4). The 600-m-wide Yingjiang shear zone is composed of mylonized biotite-plagioclase gneisses, biotite-sillimanite gneisses and granitic gneisses. The foliation generally dips 70–80° to the west but locally dips to SE (Fig. 4). The stretching lineation plunges 10–30° to the southwest (Fig. 10c). Various felsic veins are parallel to the foliation and have been boundinaged with a dextral shear sense (Fig. 10d). The Yingjiang shear zone was overprinted by normal faulting and defines the eastern boundary of the Neogene-Quaternary Yingjiang basin. Similarly, the ~500 m wide NE-striking Lianghe strike-slip shear zone is composed of steeply dipping mylonites and paragneisses. To the northeast, the Lianghe shear zone merges with a SE-dipping normal fault that bounds the Tengchong Quaternary volcanic basin (Fig. 4).

Gneisses and mylonites from the Sudian, Yingjiang and Lianghe shear zones have similar microstructures and dextral shear sense (Fig. 11). The core-mantle structure of plagioclase porphyroclasts suggests deformation under amphibolite facies conditions.

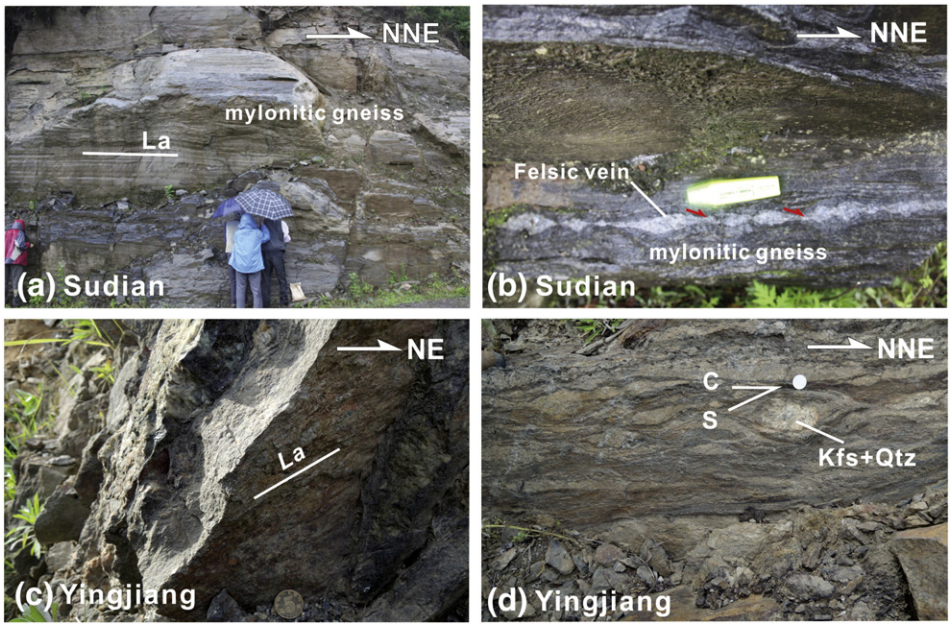

Fig. 10. Outcrop observations of (a–b) the Sudian and (c–d) Yingjiang strike-slip shear zones in the Tengchong Terrane. (a) The horizontal NNE-trending horizontal lineation and steep foliation of mylonitic gneiss, and (b) rotated asymmetric boudins of a felsic vein within mylonitic gneiss (site 27-5 near Sudian village). (c) The SW-trending subhorizontal lineation in steeply dipping foliated schist (site 16-2), and (d) S/C fabric and boundinaged felsic veins in mylonites (site 2-6).

5. Quartz fabrics of ductile shear zones

The crystallographic preferred orientation (CPO) of quartz in mylonites and gneisses from the Donghe Detachment and the Gaoligong and Nabang shear zones was determined using the electron backscatter diffraction (EBSD) technique on a scanning electron microscope JEOL JSM-5610LV in the State Key Laboratory of Continental Tectonics and Dynamics, Institute of Geology, Beijing. Thin sections were cut parallel to the structural XZ plane (X – parallel to the lineation, Y – parallel to foliation and normal to lineation, and Z – normal to foliation). The pole figures were plotted using the program of Mainprice (1990). Experimental details are given in Xu et al. (2009).

5.1. Quartz fabrics from the Donghe Detachment

Eight samples from the Donghe Detachment were analyzed. Five felsic mylonite samples (8-1-2, 7-11-3, 7-12-2, 16-8-1, and 16-9-3) show the maximum concentration of quartz c-axes near the Y-direction and that of a-axes near the lineation (Fig. 12), which indicates the dominant activation of prism <a> slip. In contrast, mylonite samples 16-7-1 and 28-3-1 display the activation of prism [c] slip, which is characterized by a girdle of a-axes normal to the lineation and a point maximum of c-axes subparallel to the lineation. In addition, granitic gneiss 28-5-1 with magmatic fabrics develops the symmetric basal <a> slip with a girdle of c-axes normal to the foliation and a single a-axes maximum parallel to the lineation, reflecting constriction at low temperature. Hence, ductile shearing in the Donghe Detachment is dominated by deformation at medium-to-high temperature (400–650 °C) (Blumenfeld et al., 1986; Mainprice et al., 1986; Schmid and Casey, 1986). The asymmetric quartz CPO from mylonite samples supports the top-to-NE or top-to-the-north shear sense interpreted at outcrops.

5.2. Quartz fabrics from the Gaoligong and Nabang shear zones

The asymmetric quartz fabrics of four felsic mylonites from the Gaoligong strike-slip shear zone show a dextral shear sense (Fig. 13a), which is consistent with observations at outcrops and in thin sections (Fig. 8). Quartz c-axes of sample 8-4-3 form a girdle normal to the lineation, with the maximum concentration near the Y direction and a sub-maximum near the Z direction, while a-axes yield a point maximum subparallel to the lineation. This is a mixed pattern for low-temperature basal <a> slip and medium-temperature prism <a> slip under simple shear (e.g., Barth et al., 2010). In contrast, mylonite samples 8-5-2 and 8-5-3 develop the basal <a> slip characterized by a point maximum of c-axes near the Z direction and a girdle of a-axes subparallel to the foliation. Mylonite 8-5-5 shows a typical prism <a> slip alone. Therefore the Gaoligong shear zone was formed by consistent dextral shearing under 300–500 °C.

The asymmetric quartz CPO of four felsic mylonites from the Nabang shear zone also yields a dextral slip (Fig. 13b), consistent with outcrop and thin section observations (Fig. 9). Samples 4-3-5 and 4-4-6 contain a c-axis maximum of quartz around the Y direction and a single a-axes maximum near the lineation, which can be explained by the dominant activation of prism <a> slip under medium temperature (400–650 °C) (e.g., Schmid and Casey, 1986; Stipp et al., 2002). However, in samples 4-5-1 and 4-4-10, quartz c-axes form a point maximum subparallel to the lineation with a girdle of a-axes normal to the lineation, which is the typical prism [c] slip at high temperature (>650 °C) and possibly hydrous conditions (Blumenfeld et al., 1986; Mainprice et al., 1986). Therefore, the quartz CPO of the Nabang shear zone records dextral shearing at medium to high temperature, which is consistent with widespread anatexis in high strain zones, as well as lobate grain boundaries of quartz and myrmekite growth of K-feldspar (Fig. 9).

6. Zircon U-Pb geochronology

To unravel the temporal relationship between magmatism and ductile deformation, we determined zircon U-Pb ages of 8 mylonites and mylonitic gneisses by LA-ICP-MS at the State Key Laboratory of Geological Processes and Mineral Resources, China University of Geosciences (Wuhan) (Table S1). The apparent crystallization temperatures of zircon were also calculated by using the Ti-in-zircon thermometer (Watson et al., 2006) and assuming the TiO_2 activity of 1.0 (Table S2). Experimental details are given in Appendix 1.

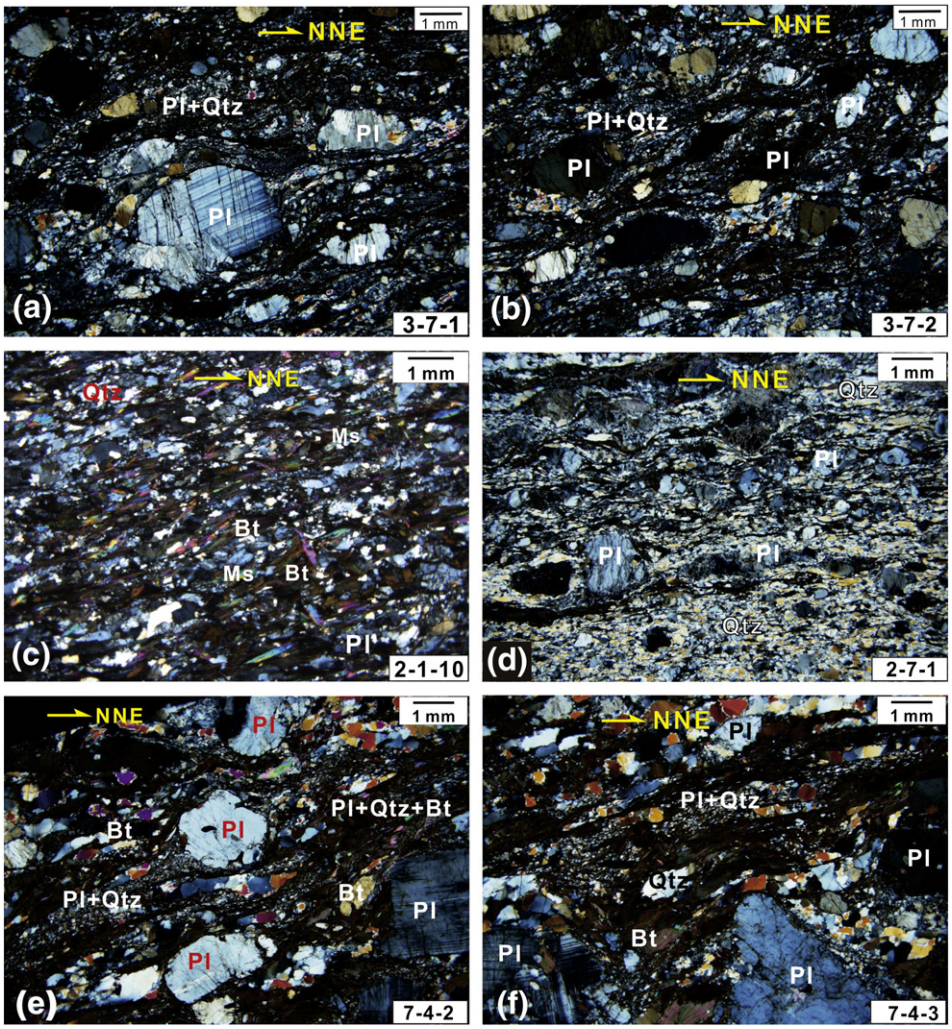

Fig. 11. Microphotographs of gneisses and mylonites from the (a–b) Sudian, (c–d) Yingjiang and (e–f) Lianghe strike-slip shear zones, showing a dextral shear sense. (a–b) σ-type plagioclase porphyroclasts with core-mantle structure from granitic mylonites in the Sudian shear zone. (c) S-C fabric and (d) σ-type plagioclase porphyroclasts from felsic mylonites in the Yingjiang shear zone. (e) σ-type plagioclase porphyroclasts and mica fish, and (f) S-C fabric in shear bands from granitic mylonites in the Lianghe shear zone. XZ thin sections, cross polarized light.

6.1. Zircon U-Pb ages of the Donghe Detachment

Six samples of the Donghe Detachment were collected from the western Mangshi area (Fig. 3). Samples 7-10-2, 28-6-5 and 28-7-4 are foliated granites with magmatic fabrics. Their zircons are euhedral to subhedral, long or stubby prismatic, and show typical oscillatory igneous zoning (Fig. 14a). Sample 7-10-2 was collected from a small granitic intrusion within the mylonitic basement rocks. Fourteen grains of sample 7-10-2 yield a mean $^{206}Pb/^{238}U$ age of 50.5 ± 0.6 Ma, with the mean square of weighted deviation (MSWD) of 0.19 (Fig. 15a). Sample 28-6-5 represents an early foliated granite intrusion and sample 28-7-4 is from a small granitic vein intruding sample 28-6-5. The weighted mean $^{206}Pb/^{238}U$ ages give the crystallization age at 108 ± 1 Ma (MSWD = 0.25, 15 analyses) for sample 28-6-5 (Fig. 15b), and at 55.0 ± 0.5 Ma (MSWD = 0.36, 16 analyses) for sample 28-7-4 (Fig. 15c). The ages of the three granite samples confirm magmatism in the early Cretaceous and early Eocene in the eastern Tengchong Terrane.

Sample 27-6-3 is an undeformed felsic vein with chilled contact against the flat-lying mylonites (Fig. 5e). Its zircon grains are euhedral and prismatic, with an irregular core and a relatively thin rim in CL images (Fig. 14a) and high Th/U ratios of 1.26-2.35 (Table S1), which indicate metamorphic overgrowth. Because the zircon rims of sample 27-6-3 are very thin, the LA-ICP-MS analyses may overlap the inherited core and the overgrowth rims of zircons (Fig. 14a). A mean $^{206}Pb/^{238}U$ age of 35.4 ± 0.5 Ma (MSWD = 0.115) is determined from 13 analyses (Fig. 15d). The temperature of zircon crystallization is estimated as ~676 °C for sample 27-6-3 from the Ti-in-zircon thermometer, implying zircon growth under a late hydrothermal event (Fig. 16a) (Claoué-Long et al., 1995; Hoskin and Schaltegge, 2003). Because this felsic vein cuts through the subhorizontal foliation of mylonites, ductile shearing along the Donghe Detachment should precede 35 Ma.

Sample 28-5-5 represents foliated granite from the upper part of a granitic sheet (Fig. 5f) that intruded into mylonitic orthogneisses, and sample 28-5-6 is a sheared leucogranite vein within this granitic sheet. Both samples show subhorizontal foliation consistent with the Donghe Detachment. Zircons from sample 28-5-5 are euhedral and have fine-scale oscillatory igneous zoning, with length/width ratios from 1.2 to 2.0 (Fig. 14a). The U-Pb dating for zircons obtains a mean $^{206}Pb/^{238}U$ age of 118 ± 1 Ma (MSWD = 1.0, 11 analyses) for sample 28-5-5 (Fig. 15e). In contrast, zircons from sample 28-5-6 are euhedral and show a core-rim structure (Fig. 14a). The cores are irregular with gray and homogeneous CL features, whereas the rims are homogenous and preserve crystal shapes. The zircon CL images of sample 28-5-6 indicate metamorphic growth of zircon under high temperature (Williams, 1998), which are consistent with the estimated zircon crystallization temperature of 764 °C (Fig. 16b). 9 analyses on zircon rims

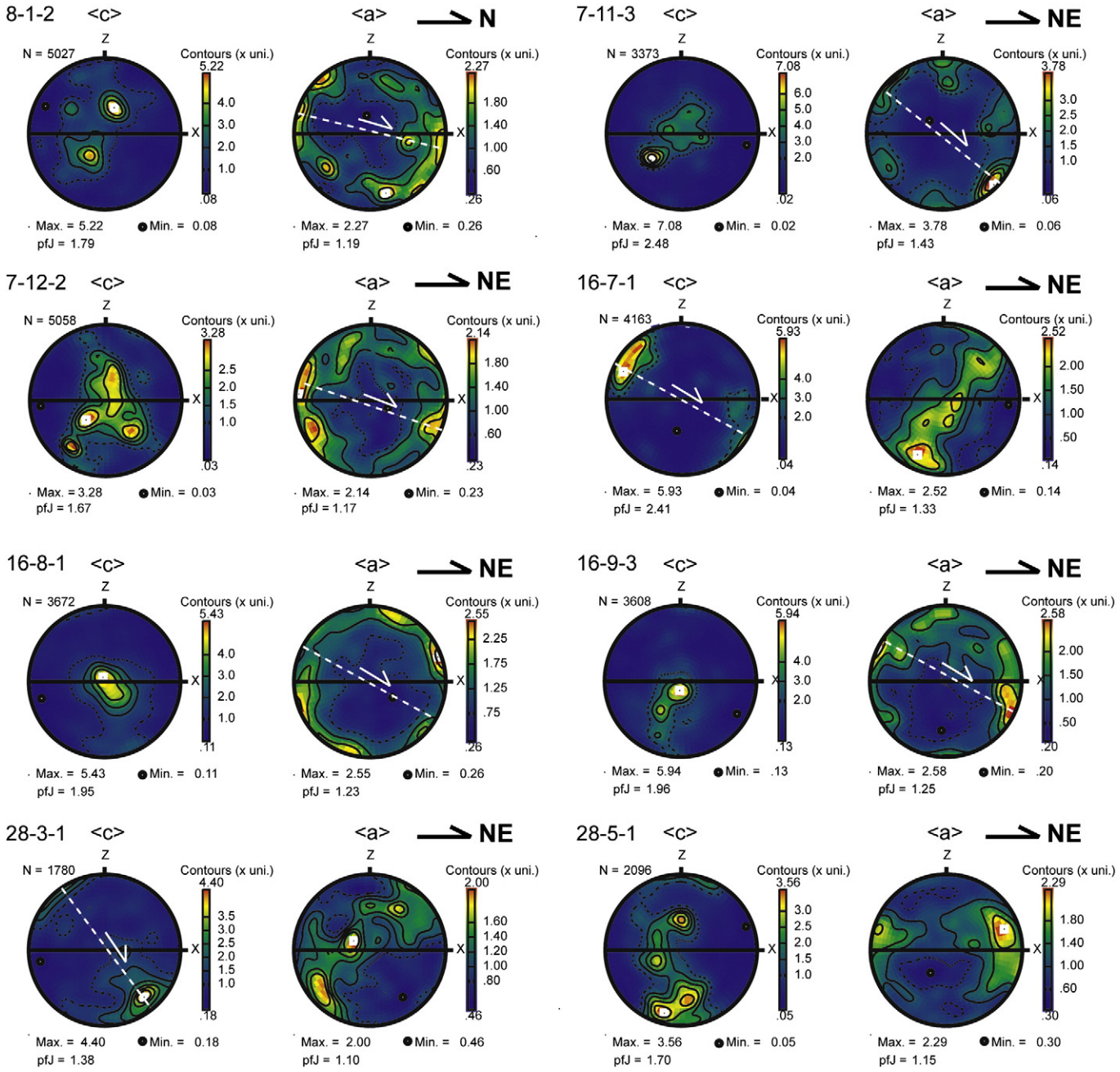

Fig. 12. Pole figures of quartz c- and a-axes for mylonites and mylonitic gneisses from the Donghe Detachment. Lower hemisphere, equal area projection. The contours at multiples of a uniform distribution are plotted. Structural directions: X – parallel to the lineation, Z – normal to the foliation. N: number of data points; pfJ: texture index. The thick arrow on the upper left corner indicates the trending of the lineation at outcrops, while dashed line and thin arrow on pole figures presumably represent the inferred slip plane and shear sense, respectively.

yield a mean $^{206}Pb/^{238}U$ age of 30.1 ± 0.4 Ma (MSWD = 0.48) for sample 28-5-6 (Fig. 15f), suggesting high-temperature deformation of the leucogranite vein at 30 Ma.

6.2. Zircon U-Pb ages of the Nabang strike-slip shear zone

Samples 4-1-5, 4-3-1, 4-4-9 and 4-5-5 are from the Nabang strike-slip shear zone near the Nabang village (Fig. 3). Mylonitic hornblende-bearing granite gneiss 4-1-5 delivered light-brown, irregular, stubby zircons. The zircon grains are 100–180 μm long, with length/width ratios from 1 to 1.5. They are homogeneous in CL images (Fig. 14b) and show high Th/U ratios of 1.35–2.85 (Table S1). The featureless zircon grains with abnormally high Th/U ratios can be attributed to growth of new zircon grains during metamorphism (e.g., Liu et al., 2015; Williams, 1998). Thirteen analyses for sample 4-1-5 yield a weighted mean $^{206}Pb/^{238}U$ age of 41.0 ± 0.8 Ma with MSWD = 2.0 (Fig. 15g).

Sample 4-3-1 was collected from a mylonitic amphibolite vein. Its zircon grains are light-brown, short prismatic, partly irregular in shape, with low Th/U ratios (most between 0.06 and 0.51 in Table S1). Some zircon grains are homogeneous, and some show a core-rim texture with a homogeneous rim in CL images (e.g., spots 7 and 8 of 4-3-1) (Fig. 14b). The similar U-Pb ages of the featureless zircon grains and the homogeneous rims suggest a metamorphic origin of zircons from the latest high-temperature episode. Twelve analyses for sample 4-3-1 reveal a weighted mean $^{206}Pb/^{238}U$ age of 28.4 ± 0.4 Ma (MSWD = 0.19) (Fig. 15h). Hence this mafic vein experienced mylonization and coeval high-temperature metamorphism at 28 Ma.

In contrast, zircons from hornblende-bearing granite gneisses 4-4-9 and 4-5-5 are light-brown, euhedral to subhedral, and prismatic. They

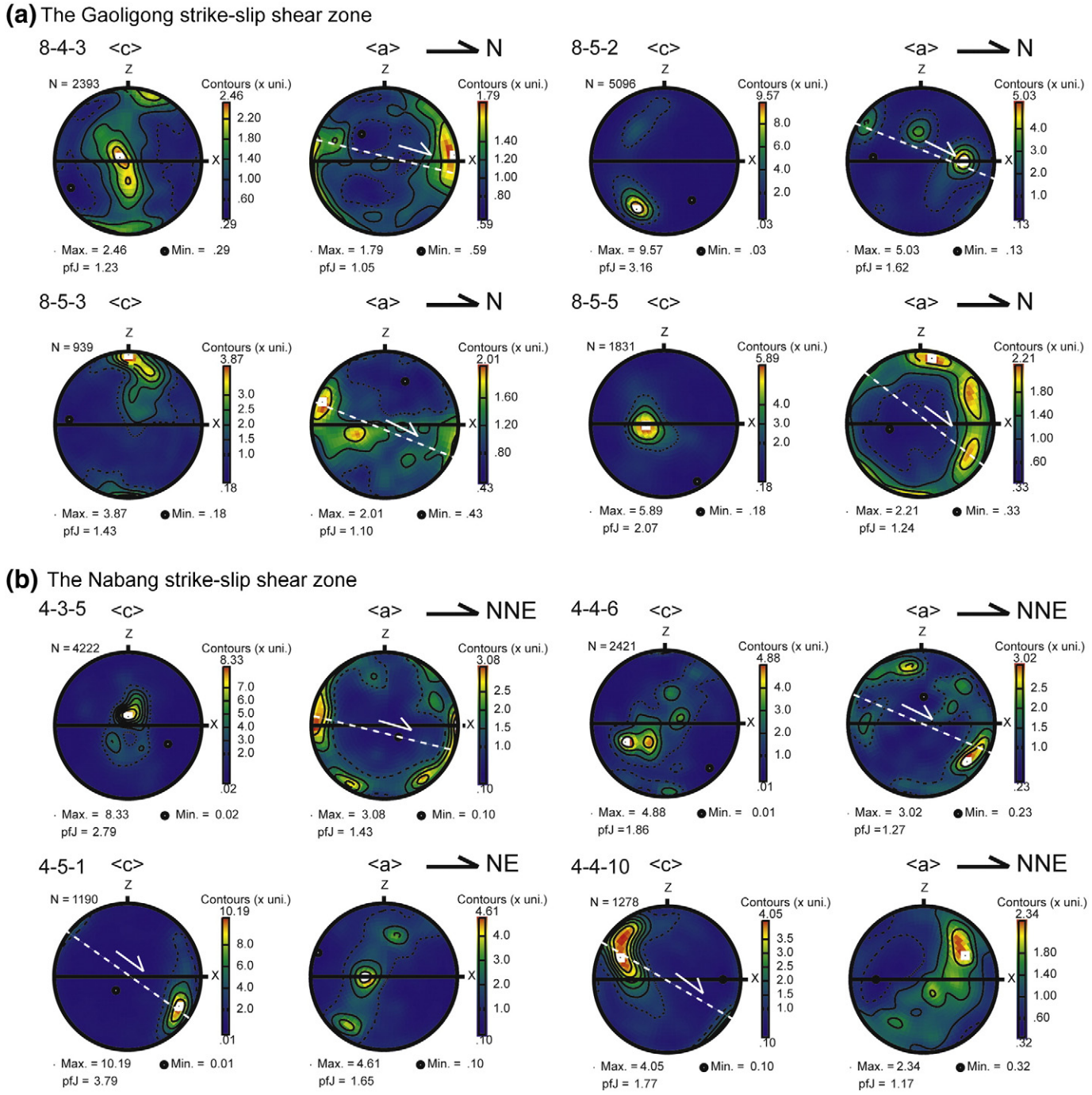

Fig. 13. Pole figures of quartz c- and a-axes from mylonites in (a) the Gaoligong strike-slip shear zone and (b) the Nabang strike-slip shear zone. Description is same as Fig. 12.

are between 120 and 250 μm long with length/width ratios from 1.2 to 2.5, and display concentric oscillatory zoning typical for an igneous origin (Fig. 14b). The consistent mean weighted $^{206}Pb/^{238}U$ ages of samples 4-4-9 (53.5 ± 0.5 Ma, MSWD = 0.26, 17 analyses) (Fig. 15i) and 4-5-5 (53.8 ± 0.7 Ma, MSWD = 0.08, 17 analyses) (Fig. 15j) demonstrate a magmatic event at ~54 Ma. The estimated temperature of zircon from Ti-in-zircon thermometer is ~800 °C for sample 4-3-1, and ~750 °C for sample 4-4-9 (Fig. 16).

Samples 6-12-1 and 6-12-2 were collected from the Nabang shear zone in the Myitkyina area, north Burma (Fig. 2). Both are sheared felsic veins in amphibolites, and develop a concordant N–S-striking steep foliation and a horizontal stretching lineation with the surrounding amphibolites. Their zircon grains are 120–280 μm long and prismatic, with length/width ratios from 1.2 to 2.5. The euhedral to subhedral oscillatory zoning of zircon in CL images indicates crystallization of the felsic veins (Fig. 14b). A mean $^{206}Pb/^{238}U$ age is determined as 43.7 ± 0.4 Ma (MSWD = 1.9, 16 analyses) for sample 6-12-1 (Fig. 15k), and 40.5 ± 0.2 Ma (MSWD = 1.7, 15 analyses) for sample 6-12-2 (Fig. 15l). The crystallization ages of the syn-kinematic felsic veins indicate that the Nabang shear zone was subjected to ductile shearing later than 41 Ma.

7. $^{40}Ar/^{39}Ar$ thermochronology

To constrain the cooling history of the Tengchong Terrane, we determined $^{40}Ar/^{39}Ar$ ages of biotite, muscovite and hornblende from

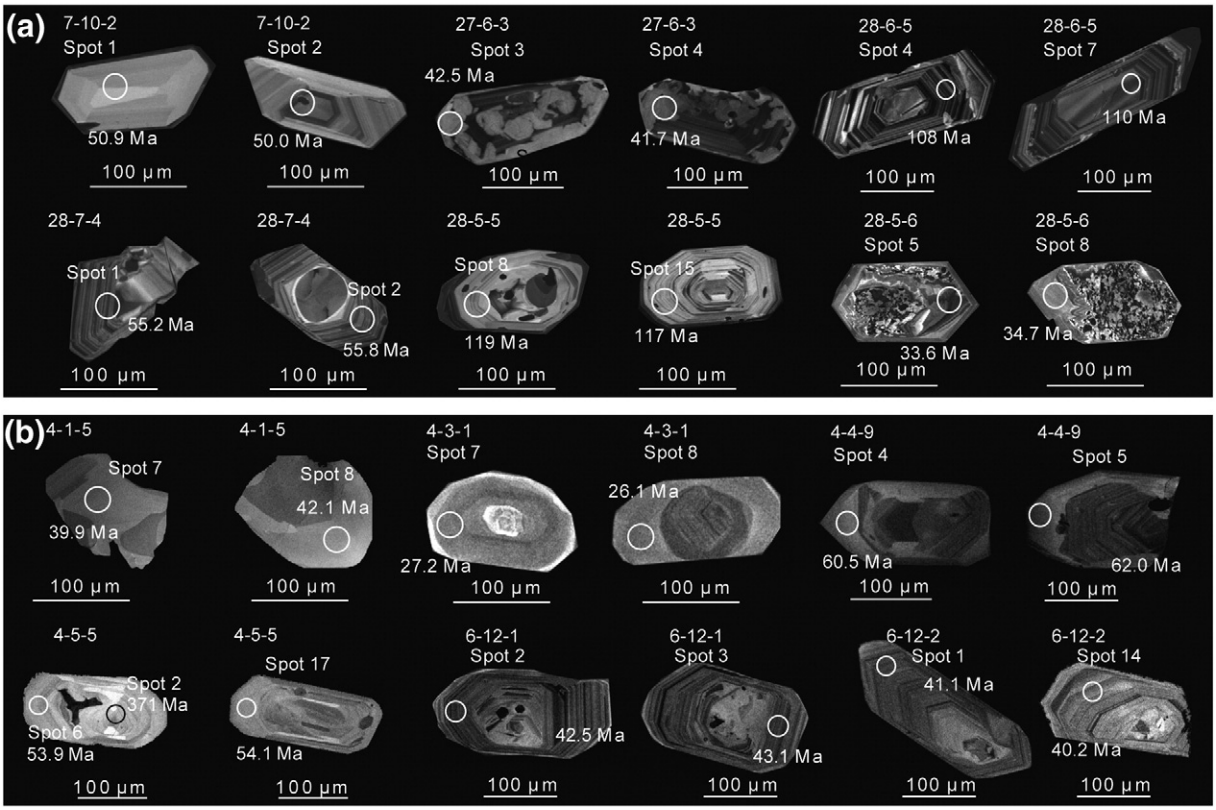

Fig. 14. Cathodoluminescence images of representative zircons from (a) the Donghe Detachment, and (b) the Nabang strike-slip shear zone.

mylonites and gneisses in the Donghe Detachment, the Gaoligong, Lianghe and Nabang strike-slip shear zones at Institute of Geology, Chinese Academy of Geological Sciences in Beijing. The experimental details are given in Appendix 1.

Fig. 3 and Table S3 show sample locations, $^{40}Ar/^{39}Ar$ ages of study minerals and uncertainties of 2σ level for 11 samples from the Donghe Detachment. Mylonitized granite gneiss 7-9-5 is from the eastern margin of the Donghe pluton, whereas mylonitic gneisses 7-12-5 and 7-14-3 are from the flat-lying mylonite zone. $^{40}Ar/^{39}Ar$ dating of biotite provides the similar plateau ages: 23.05 ± 0.17 Ma (MSWD = 2.80) for sample 7-9-5 (Fig. 17a), 23.0 ± 0.16 Ma (MSWD = 2.66) for sample 7-12-5 (Fig. 17b), and 23.6 ± 0.36 Ma (MSWD = 0.23) for sample 7-14-3 (Fig. 17c). In contrast, the $^{40}Ar/^{39}Ar$ age of biotite is 15.77 ± 0.21 Ma (MSWD = 1.17) for a mylonitic Pl-Qtz-Bt gneiss 8-1-6 near Longling County (Fig. 17d).

To unravel the relationship between the cooling history of the Donghe pluton and activation of the Donghe Detachment, we performed $^{40}Ar/^{39}Ar$ dating on the same samples as for U-Pb zircon dating (Fig. 3). The $^{40}Ar/^{39}Ar$ plateau age of hornblende of sample 28-5-5 is 22.33 ± 0.27 Ma (MSWD = 2.80) (Fig. 17e), slightly older than the muscovite $^{40}Ar/^{39}Ar$ age of 19.28 ± 0.24 Ma (MSWD = 0.74) for sample 28-5-6 (Fig. 17f). Sample 27-6-10 was collected next to the felsic vein of sample 27-6-3 (Fig. 5e). The $^{40}Ar/^{39}Ar$ plateau age of hornblende is 29.8 ± 0.3 Ma for sample 27-6-10 (Fig. 17g), slightly younger than the crystallization age (35.4 ± 0.5 Ma from zircon U-Pb dating) of the felsic vein.

In addition, the $^{40}Ar/^{39}Ar$ ages of biotite are: 22.25 ± 0.32 Ma (MSWD = 2.0) for sample 28-6-3 (Fig. 17h), 22.92 ± 0.22 Ma (MSWD = 1.3) for sample 28-6-5 (Fig. 17i), 23.90 ± 0.22 Ma (MSWD = 1.09) for sample 28-6-7 (Fig. 17j), and 24.51 ± 0.38 Ma (MSWD = 1.3) for sample 28-7-4 (Fig. 17k). The consistent $^{40}Ar/^{39}Ar$ ages of biotite from different samples at site 28-6 confirm high data quality.

Five samples were collected from the strike-slip shear zones in the Tengchong Terrane (Fig. 3 and Table S4). The $^{40}Ar/^{39}Ar$ ages of biotite yield 19.2 ± 0.1 Ma (MSWD = 0.75) for mylonitic granite 8-7-1 from the Gaoligong shear zone (Fig. 18a), and 35.2 ± 0.3 Ma (MSWD = 1.65) for mylonite 7-4-4 from the Lianghe shear zone (Fig. 18b). In addition, $^{40}Ar/^{39}Ar$ ages of hornblende from three mylonitic gneisses in the Nabang shear zone reveal amphibolite facies metamorphism at 21.7 ± 0.3 Ma (MSWD = 2.84) for sample 4-1-5 (Fig. 18c), 19.5 ± 0.4 Ma (MSWD = 3.41) for sample 4-3-1 (Fig. 18d), and 33.0 ± 0.6 Ma (MSWD = 5.49) for sample 4-5-5 (Fig. 18e).

8. Discussion

8.1. Timing of ductile shear zones in the Tengchong Terrane

Microstructures and quartz fabrics indicate that the Donghe Detachment and the Nabang strike-slip shear zone were mid-crustal shear zones active at 350–650 °C, while the Gaoligong strike-slip shear zone was activated at slightly lower metamorphic conditions (350–500 °C). The coupled U-Pb and $^{40}Ar/^{39}Ar$ dating schemes provide important information on timing of these ductile shear zones. The ages of magmatic zircon from syn- and post-kinematic intrusions constrain the initiation and cessation of ductile shearing, respectively, while zircon overgrowth rims in mylonites and synkinematic intrusions record metamorphism and the coeval ductile shearing. Because the closure temperatures of K-Ar system in hornblende, muscovite and biotite of natural samples are generally at 530 ± 40 °C, ~425 °C, and 280 ± 40 °C, respectively (Harrison, 1981; Harrison et al., 1985, 2009), $^{40}Ar/^{39}Ar$ ages of hornblende and muscovite constrain the ages of ductile deformation under medium temperature, and $^{40}Ar/^{39}Ar$ ages of biotite should be synchronous with the change from ductile to brittle deformation (Parrish, 2001).

The undeformed felsic vein (sample 27-6-3) cutting the mylonitic foliation contains zircons grown in a late hydrothermal event at 35.4 ± 0.5 Ma, implying initiation of the Donghe Detachment before 35 Ma. The $^{40}Ar/^{39}Ar$ age of hornblende from nearby mylonites is

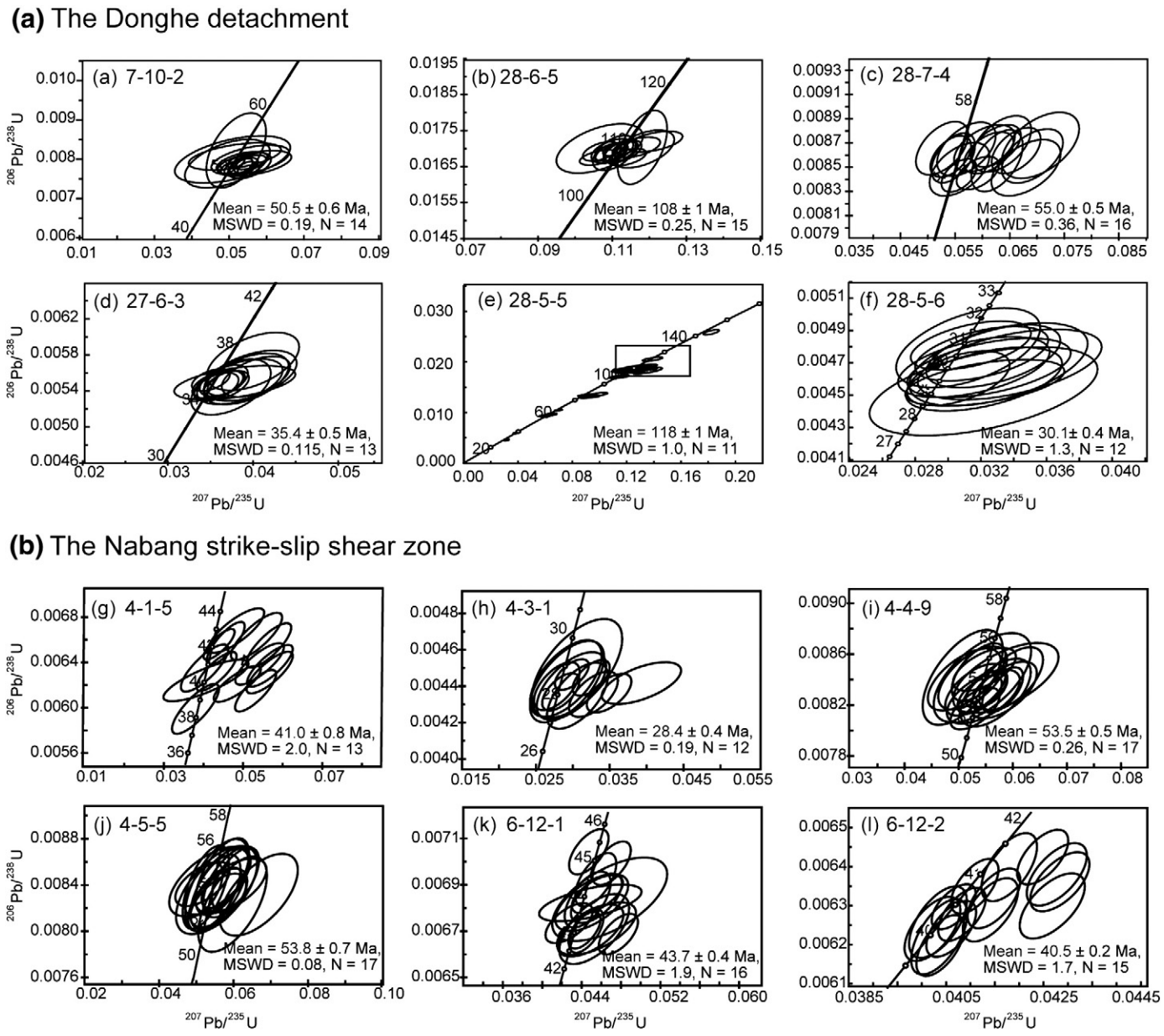

Fig. 15. Concordia diagram of the LA-ICP-MS U-Pb zircon dating results for (a) the Donghe Detachment, and (b) the Nabang strike-slip shear zone.

29.8 ± 0.3 Ma (sample 27-6-10). Therefore, the felsic veins have locally heated surrounding mylonites and gneisses, and probably re-activated or facilitated ductile shearing in the Donghe Detachment.

A syn-kinematic leucogranite vein (sample 28-5-6) has zircon U-Pb age of 30.1 ± 0.4 Ma and muscovite $^{40}Ar/^{39}Ar$ age of 19.3 ± 0.2 Ma, suggesting that the Donghe Detachment was subjected to syn-kinematic partial melting at 30 Ma and then rapidly exhumed. $^{40}Ar/^{39}Ar$ cooling ages of biotite range from 22.3 to 24.5 Ma for gneisses and mylonites from the Donghe Detachment, including high-grade metamorphic basement rocks (samples 7-12-5 and 7-14-3), early Cretaceous granites (samples 28-5-5 and 28-6-5) and Eocene granites (sample 28-7-4). The $^{40}Ar/^{39}Ar$ ages of biotite overlap with the hornblende $^{40}Ar/^{39}Ar$ age of 22.3 ± 0.3 Ma for the foliated granite 28-5-5, implying fast cooling around 22 Ma. However, the mylonitic gneiss 8-1-6 yields biotite $^{40}Ar/^{39}Ar$ age of 15.8 ± 0.2 Ma, comparable with $^{40}Ar/^{39}Ar$ ages of 14–16 Ma for biotite and muscovite from granitic mylonites in the Gaoligong strike-slip shear zone (Lin et al., 2009; Wang et al., 2006; Zhang et al., 2012) (Fig. 3). Therefore ductile shearing of the Donghe Detachment occurred from >35 to 16 Ma, with fast cooling between 30 and 22 Ma.

It is notable that mylonites in the Gaoligong strike-slip shear zone have hornblende $^{40}Ar/^{39}Ar$ ages of 32 Ma and biotite $^{40}Ar/^{39}Ar$ ages of 15-28 Ma (Lin et al., 2009; Wang et al., 2006; Zhang et al., 2012; this study). Therefore, initiation of the dextral Gaoligong strike-slip shear zone lagged behind the Donghe Detachment, but the two shear zones were active simultaneously under medium to low-grade metamorphism. The youngest biotite $^{40}Ar/^{39}Ar$ ages of 10–11 Ma from weakly deformed leucogranites and protomylonites suggest long-lasting deformation in the Gaoligong shear zone (Zhang et al., 2012).

To the west, zircon U-Pb ages of granite gneisses and leucogranites in the Nabang strike-slip shear zone reveal regional magmatism from 66 to 52 Ma (Ma et al., 2013; Xu et al., 2012; this study). The sheared felsic veins in mylonitic amphibolites contain magmatic zircon of 41-44 Ma (samples 6-12-1 and 6-12-2 in the Myitkyina area in Fig. 2), while a mylonitic hornblende-bearing granite gneiss shows zircon overgrowth at 41 Ma under high-grade metamorphism (sample 4-1-5 near

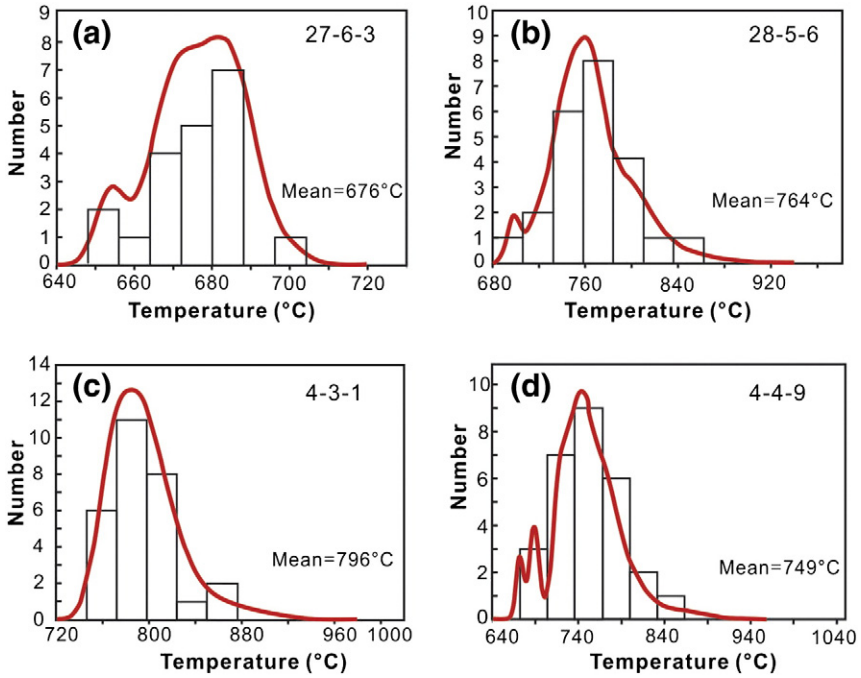

Fig. 16. Formation temperature of zircon estimated from Ti-in-zircon thermometry.

Nabang village in Fig. 3). As discussed above, the former constrains ductile shearing as younger as 41 Ma, whereas the latter dates syn-kinematic shearing. We thus conclude that the coeval deformation and high-temperature metamorphism began at 41 Ma in the Nabang shear zone. The mylonitic amphibolite vein (sample 4-3-1) was subjected to granulite facies metamorphism at 28.4 ± 0.4 Ma (U-Pb age of metamorphic zircon rims, Fig. 15h) and then retrogressed to amphibolite facies at 19.5 ± 0.4 Ma (hornblende $^{40}Ar/^{39}Ar$ age, Fig. 18d). Qi et al. (2015) reported zircon U-Pb age of 19.7 Ma for a dextrally sheared gneissic granodiorite from the Nabang shear zone. Combined with widespread syn-kinematic felsic veins and migmatites (Fig. 9) and occurrence of high-temperature quartz fabrics (Fig. 13), synkinematic partial melting in the Nabang shear zone spanned from 41 Ma to 20 Ma. This timing range covers hornblende $^{40}Ar/^{39}Ar$ ages of 19–33 Ma and biotite $^{40}Ar/^{39}Ar$ age of 28 Ma for foliated metamorphic rocks in the Nabang shear zone (Fig. 3) (Ji et al., 2000; Wang et al., 2006; this study). The Nabang dextral strike-slip shear zone was thus active as early as 41 Ma and continued to 19 Ma, with high-temperature metamorphism and fast cooling.

We obtained only one biotite $^{40}Ar/^{39}Ar$ age of 35.2 ± 0.3 Ma for the Lianghe strike-slip shear zone (sample 7-4-4 in Fig. 18b). It suggests that ductile shearing was terminating by 35 Ma. The mapped gradual variation of the foliation from low-angle mylonites and gneisses to steeply dipping strike-slip shear zones (Fig. 4) suggests that coeval shearing in the detachments and in the strike-slip shear zones bounded the Donghe gneiss dome. Therefore, we interpret the Lianghe dextral strike-slip shear zone to have been activated with the Donghe Detachment before 35 Ma, but it was soon abandoned when strike-slip faulting became concentrated on the Gaoligong and Nabang shear zones. No geochronological data exist for the Yingjiang and Sudian strike-slip shear zones. Given their similar structure as that of the Lianghe shear zone, we also interpret them as short-lived, late Eocene ductile shear zones. Additional geochronological investigations are needed to test our interpretation.

Timing of shear zones is very important for our understanding of deformation mechanisms of the continental lithosphere during the Indo-Eurasia convergence. The 'tectonic escape' model emphasizes the controlling role of strike-slip faulting in extrusion of rigid blocks from central Tibet towards South China and Indochina (Leloup et al., 2001; Tapponnier and Molnar, 1976; Tapponnier et al., 1986). In contrast, assuming the continental lithosphere as a continuous medium, the 'thin viscous sheet' model regards diffuse crustal thickening as the predominant mechanism accommodating continental convergence, with strike-slip faulting as a subsidiary and relatively recent result (England and Houseman, 1986; Houseman and England, 1986). Clearly, the strike-slip shear zones and mid-crustal detachments in the Tengchong Terrane have been active since the initiation of tectonic extrusion. The "extruding blocks" bounded by strike-slip shear zones, such as the Tengchong Terrane, are neither rigid as required by the 'tectonic escape' model, nor vertically coherent as in the 'thin viscous sheet' model.

8.2. Magmatism in the Tengchong Terrane

A critical argument for crustal flow in the Tibetan Plateau is widespread partial melting in the middle-lower crust, which produces significant viscosity contrast across the channel boundaries (e.g., Clark and Royden, 2000; Godin et al., 2006; Grujic, 2006). If the gneiss domes in the Tengchong Terrane were generated by crustal flow, the boundary shear zones should become rigid channel boundaries with opposite shear senses, meanwhile the core of domes should develop pervasive deformation with simultaneous migmatites and leucogranites.

Previous studies documented southwestward magmatic migration in western Yunnan with early Cretaceous (121–126 Ma) granites in the Gaoligong batholiths, late Cretaceous (68–76 Ma) granites in the Tengliang area, and Paleocene to early Eocene plutons (50–66 Ma) in the Yingjiang and Nabang areas (Fig. 19a) (Ma et al., 2013; Qi et al., 2015; Xu et al., 2012; Yang et al., 2009). However, new zircon U-Pb ages of 108–118 Ma and 50–55 Ma for granites with magmatic fabrics in the Donghe Detachment (samples 7-10-2, 28-6-5, 28-7-4 and 28-5-5 in Fig. 3) indicate that the early Cretaceous plutons in the eastern Tengchong Terrane were overprinted by early Eocene magmatism. Granites from the Guyong pluton yield biotite $^{40}Ar/^{39}Ar$ ages of 65–66 Ma and 50–52 Ma (Dong et al., 2006). Combined with zircon U-Pb ages of 72–77 Ma and 53 Ma for granites, the late Cretaceous Guyong pluton was also intruded by early Eocene granites, and then cooled down quickly. Given the lack of deformation within the plutons and the magmatic fabric coherent with the foliation of flat-lying detachments, the granite plutons of different ages in the Tenchong Terrane should have been crystallized and rheologically strong before initiation

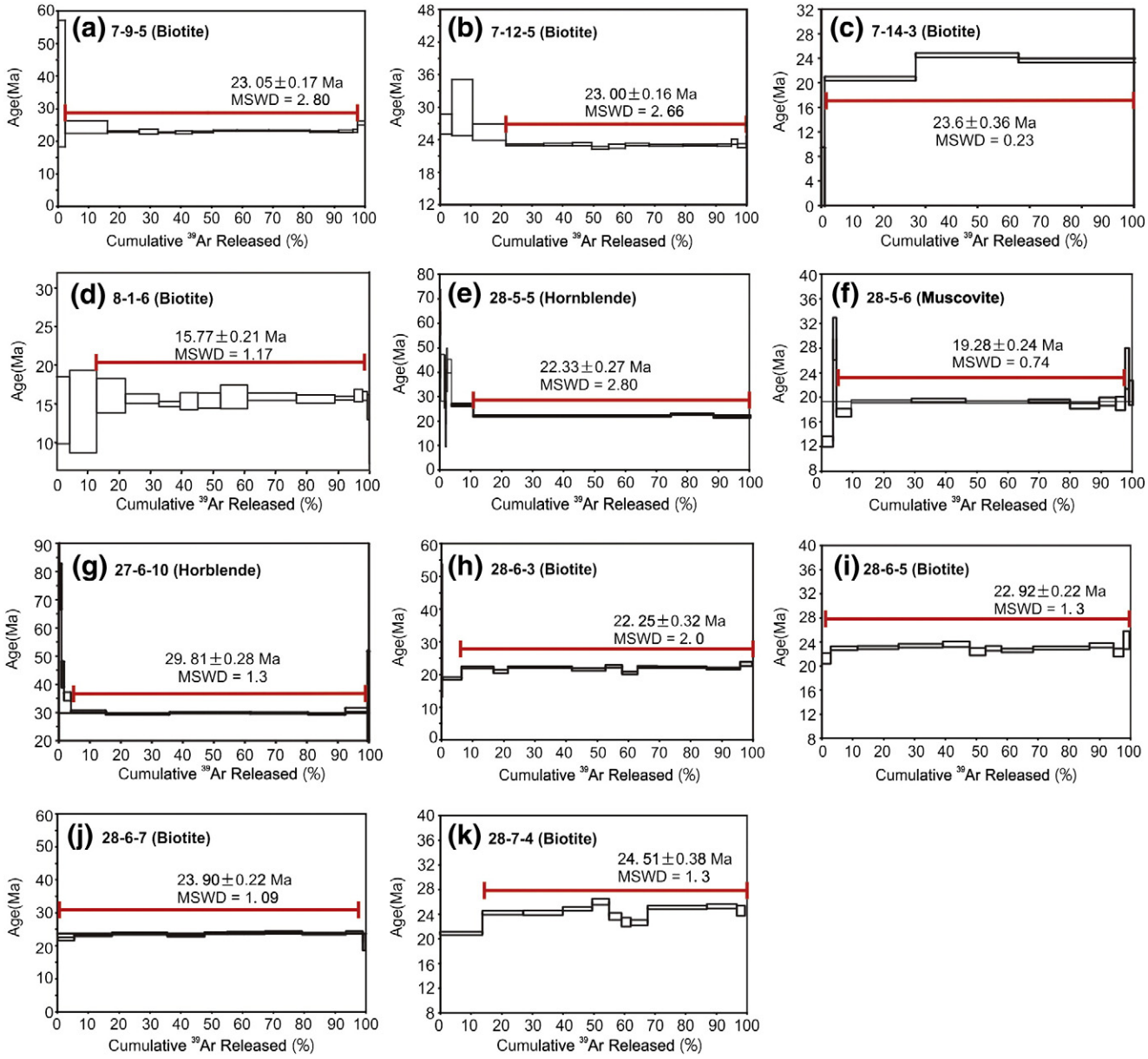

Fig. 17. $^{40}Ar/^{39}Ar$ plateau ages of biotite, muscovite and hornblende from samples in the Donghe Detachment.

of their boundary shear zones in the late Eocene. In that case, deformation was concentrated on the weak zones of the rheologically anisotropic crust (Fig. 19b), which cannot be fit by channel flow or diapiric flow of weak crustal material.

K-feldspar $^{40}Ar/^{39}Ar$ ages of 41–43 Ma for Guyong monzogranites (Dong et al., 2006) are same as 40–42 Ma ages of intraplate-type mafic dykes in the Gaoligong belt and the Lianghe area (Xu et al., 2009). Because a thin lithosphere (<80 km) is inferred from basalt geochemistry, and this is at the time of cessation of volcanism in the Gangdese magmatic arc (Chung et al., 2005; Zhou et al., 2004), Xu et al. (2009) proposed that the Neo-Tethyan slab was broken off beneath the Lhasa Terrane at 40–45 Ma. This event also corresponds to the intrusion and related high-temperature metamorphism at 41–44 Ma in the Nabang shear zone. The temporal correlation of granitic and basaltic intrusions, high-grade metamorphism and ductile deformation suggests that breakoff of the Neo-Tethyan slab triggered intraplate magmatism from the late Eocene to early Oligocene and extension in the thermally weakened lithosphere in the Tenchong Terrane, which facilitated shearing along the detachments and the strike-slip shear zones and resulted in rapid cooling of the basement rocks and granite plutons.

8.3. Formation of gneiss domes in the Tengchong Terrane

We recognized a system of elongated Donghe, Guyong, Yingjiang and Sudian gneiss domes in the Tengchong Terrane. Different from a magmatic gneiss dome cored by synkinematic intrusions and associated with the domal-shaped foliation and radial lineation (e.g., Vanderhaeghe et al., 1999; Whitney et al., 2004), the gneiss domes in the Tengchong Terrane are cored by high-grade metamorphic rocks and pre-kinematic granite plutons, overlain by the top-to-NE detachments and bounded by NE-trending dextral strike-slip shear zones (Fig. 7 and Fig. 20). Therefore, the gneiss domes in the Tengchong Terrane belong to fault-related gneiss domes in the classification of Yin (2004). The Tengchong Terrane has been involved in clockwise rotation around the Indian indenter (Kornfeld et al., 2014a; Otofuji et al., 2010). The key question is how tectonic activity in lateral fault movement achieved rotation of continental blocks.

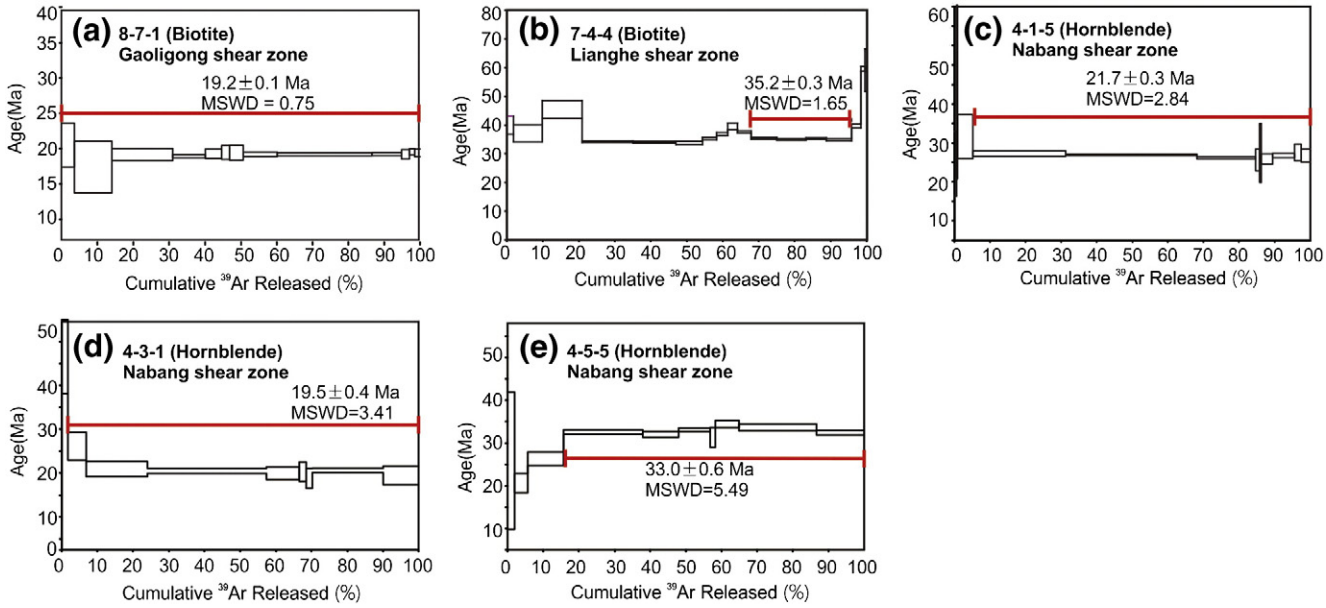

Fig. 18. $^{40}Ar/^{39}Ar$ plateau ages of biotite and hornblende from mylonitic gneisses in the Gaoligong, Lianghe and Nabang strike-slip shear zones.

The spacing of the gneiss domes in the Tengchong Terrane was controlled by the spacing of strike-slip shear zones. Burchfiel and Chen (2012) suspected that the Tengchong Terrane is an arcuate arc around vertically plunging folds due to the indentation of the Indian Plate into Eurasia, albeit without evidence. As outlined above, the newly discovered Sudian, Yingjiang and Lianghe dextral strike-slip shear zones have the same orientation, shear sense and probably same activation age as the Nabang and Gaoligong strike-slip shear zones. After 35 Ma, deformation was localized on the Nabang and Gaoligong strike-slip shear zones. Recent paleomagnetic data from ~50–35 Ma (likely ~40 Ma) mafic dykes in Yunnan province demonstrate a clockwise rotation of 87° of the Tengchong Terrane with respect to stable Eurasia, with rapid rotation between 40–30 Ma and slower rotation during the Miocene (Kornfeld et al., 2014a). Therefore, the strain geometry and temporal relationships of these strike-slip shear zones can be interpreted as vertically plunging folds formed by bending of the lithosphere around

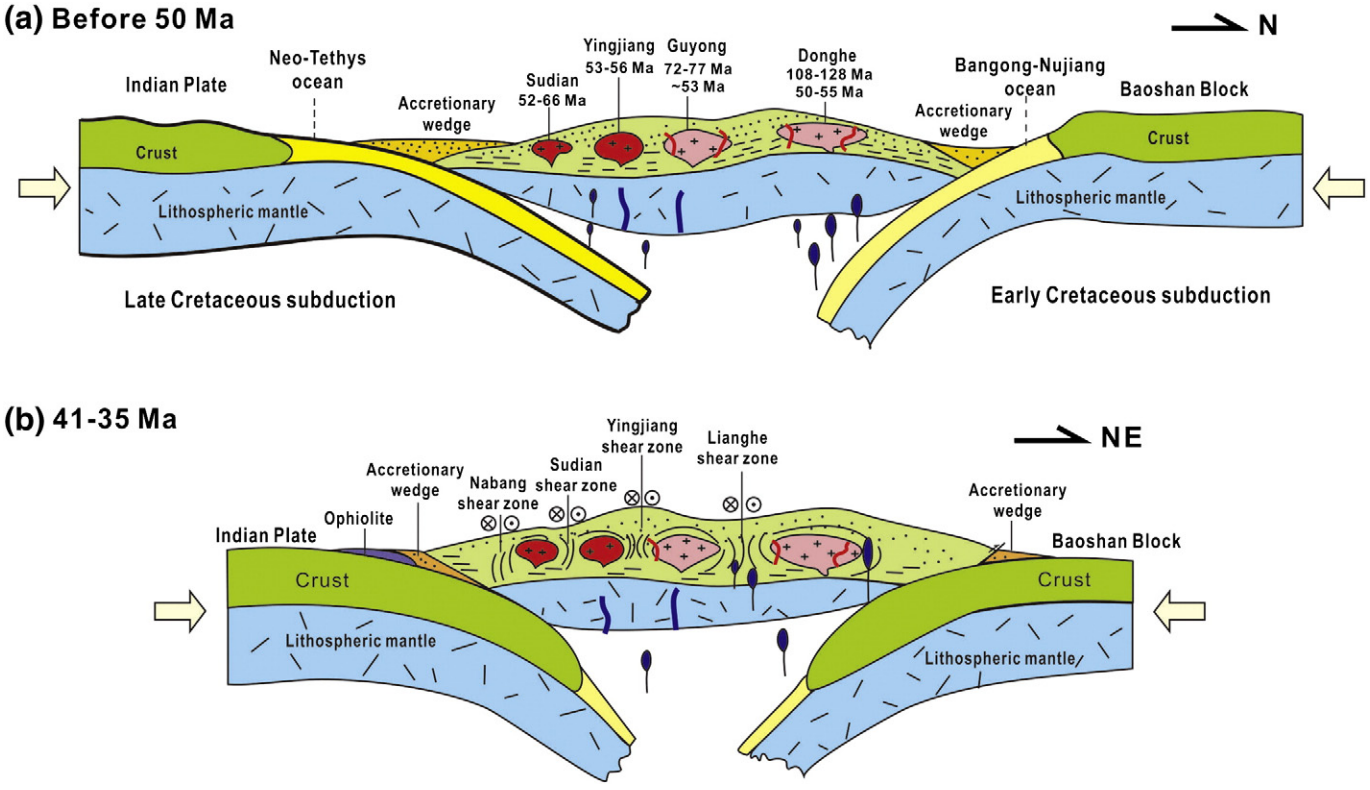

Fig. 19. Diagram for magmatism and tectonic framework of the Tengchong Terrane in the Cretaceous and the Eocene. (a) Multiple magmatism before 50 Ma due to northward subduction of the Neo-Tethyan oceanic slab and southward subduction of the Bangong-Nujiang oceanic slab; (b) Intraplate magmatism and ductile shearing along boundaries of the earlier granite plutons at 41–35 Ma.

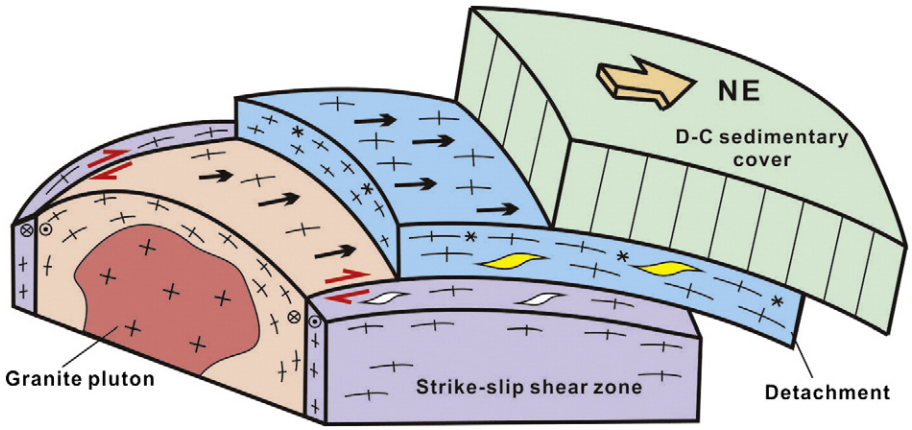

Fig. 20. Schematic view of a gneiss dome in the Tengchong Terrane showing some features: Precambrian high-grade metamorphic core with granite plutons of the early Cretaceous to early Eocene, metamorphic mantling rocks composed of flat-lying detachments with top-to-NE shear sense and dextral strike-slip shear zones, and the overlain Paleozoic sedimentary sequences.

the northeast corner of the Indian Plate since 41 Ma (Fig. 21). The Sudian, Yingjiang and Lianghe strike-slip shear zones were subordinate slip planes to accommodate the clockwise rotation of the Tengchong Terrane around the proto-eastern Himalayan syntaxis. The Kumann dextral strike-slip shear zone is probably a major slip plane of the bent Tengchong Terrane. Although the Tengchong Terrane has been long viewed as a rigid block with coherent deformation during tectonic escape (e.g., Kornfeld et al., 2014a; Replumaz and Tapponnier, 2003), the large amount of shear strain within it is sufficient to accommodate Cenozoic rotation around the syntaxis.

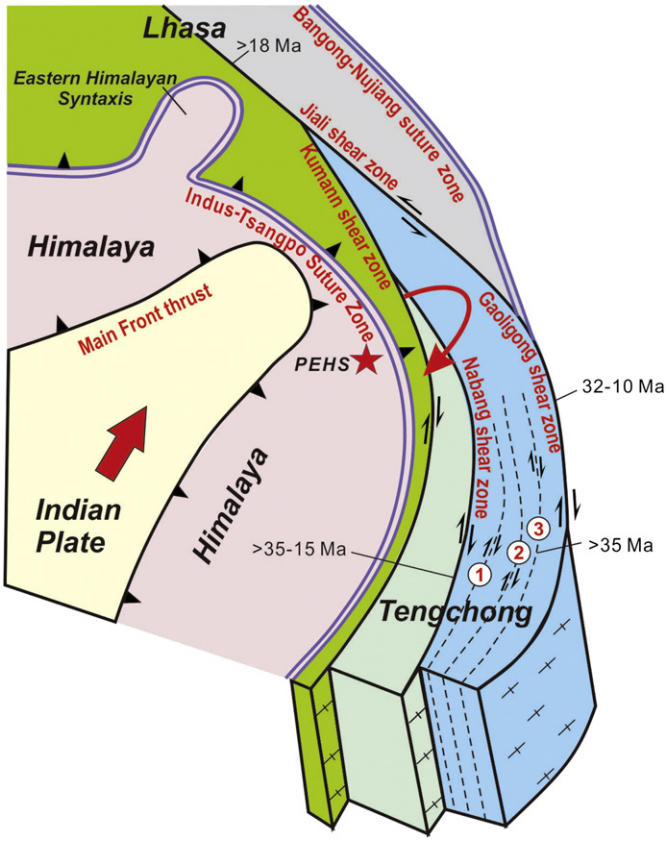

Fig. 21. A lithospheric bending model of the Tengchong Terrane. A star indicates the position of the proto-eastern Himalayan syntaxis (PEHS) at 41 Ma. Clockwise rotation of the Tengchong Terrane around the PEHS was achieved by the dextral movement along strike-slip shear zones, which separated the Tengchong Terrane into several parallel crustal slices and formed vertically plunging folds around the PEHS.

It is noteworthy that the Jiali strike-slip shear zone changed the shear sense from sinistral at >22 Ma to dextral since ~18 Ma, which linked the Jiali shear zone to the dextral Gaoligong strike-slip shear zone (Lee et al., 2003; Lin et al., 2009). Thus, the two shear zones should occur to the east and to the west of the proto-eastern Himalayan syntaxis before 18 Ma, respectively (Fig. 21). The proto-eastern Himalayan syntaxis should be located to the south of the eastern Himalayan syntaxis, which is the present-day rotation axis of Tibetan crustal materials from GPS observations (Gan et al., 2007; Zhang et al., 2004). The inferred proto-eastern Himalayan syntaxis is consistent with the reconstructed position of the northeastern point of the Indian Plate (Molnar and Stock, 2009). In addition, this model provides a possible mechanism for the counter clockwise rotation along the ITSZ (Otofuji et al., 2010). The clockwise rotation of the Tengchong Terrane before 18 Ma should occur around the proto-eastern Himalayan syntaxis, not the eastern Himalayas syntaxis as proposed by Kornfeld et al. (2014a).

The clockwise rotation of the Tengchong Terrane since the late Eocene resulted in southward displacement of lithospheric materials. However, the activation of top-to-NE and top-to-the-north detachments from the late Eocene to early Miocene indicates faster southward extrusion below the detachments, hence decoupling of the Precambrian basement from the overlying sedimentary cover. It is interesting to notice that the sinistral slip on the ARRSZ was active between 34 and 17 Ma, and reversed to dextral slip in the late Miocene and early Pliocene, which essentially coincided with spreading of the South China seafloor between 32 and 17 Ma (e.g., Gilley et al., 2003; Harrison et al., 1996; Leloup et al., 1995, 2001; Zhu et al., 2009a, 2009b). The coeval activation of the sinistral ARRSZ and the dextral Gaoligong shear zone and opening of the South China Sea is generally viewed as the onset of the continental extrusion in SE Asia (Replumaz and Tapponnier, 2003; Tapponnier et al., 1986). However, based on the occurrence of highly potassic mafic magmas in western Yunnan and northwestern Vietnam, Chung et al. (1997) claimed that an extensional regime existed in South China continental margin at 40–30 Ma, prior to the late Oligocene onset of southeastward extrusion of Indochina. Our study on earlier ductile deformation in the Tengchong Terrane provides kinematic evidence to answer how the collision-induced strain partitioned to the west of the Gaoligong shear zone prior to the tectonic extrusion of Indochina. This resolves the 'time lag' between the early Eocene magmatism and the late Oligocene deformation in SE Tibet.

Combined with new structural and geochronological data from this study, we suggest that such changes in stress regime in SE Tibet at ~18 Ma were related with the change of deformation mechanisms, i.e., from the intraplate bending around the proto-eastern Himalayan syntaxis to large-scale continental extrusion along strike-slip shear zones. The Tengchong gneiss dome system provides an example how

the mid-crustal flat-lying detachments and strike-slip shear zones work together to decouple high-grade metamorphic basement rocks from overlying sedimentary sequences during continental convergence.

9. Conclusions

Combined new structural and geochronological data allow establishing structural and temporal relationships between flat-lying detachments and strike-slip shear zones in the Tengchong Terrane.

(1) Four fault-related gneisses domes in the Tengchong Terrane are cored by high-grade metamorphic rocks and early Cretaceous to Eocene plutons. The domes are bounded by NE-trending strike-slip shear zones and by flat-lying ductile detachments with a top-to-NE or top-to-the-north shear sense. The detachments separate the hanging wall of Paleozoic sedimentary sequence from the footwall Proterozoic basement, suggesting middle crustal decoupling during indention of the Indian Plate into Asia.

(2) The Donghe Detachment (>35–15 Ma) and the Nabang strike-slip shear zone (41–19 Ma) were subjected to prolonged, nearly coeval ductile deformation under high- to low-temperature metamorphism from the late Eocene to the early Miocene. However, the Gaoligong strike-slip shear zone experienced dextral shearing under amphibolite facies to greenschist facies metamorphism at 32–10 Ma. Consistency between $^{40}Ar/^{39}Ar$ ages of hornblende from the three shear zones indicates their contemporaneity. In contrast, the newly discovered NE-trending strikes slip Sudian, Yingjiang, and Lianghe shear zones were probably active from 41 to 35 Ma.

(3) The lithosphere of the Tengchong Terrane was neither rigid nor vertically coherent during its southward extrusion and clockwise rotation. A lithospheric bending model explains the strain geometry and temporal relationships of the strike-slip shear zones. The Tengchong Terrane is composed of vertically plunging folds formed by bending of the gneiss domes and overlying sedimentary sequence around the northeast corner of the Indian Plate since 41 Ma. The intense clockwise rotation of the Tengchong Terrane was accommodated by strike slip along the Sudian, Yingjiang, Lianghe and Nabang shear zones before 35 Ma, and the subsequent localized movement along the Nabang and Gaoligong strike-slip shear zones until the early Miocene. Coeval activation of the flat-lying detachments and strike-slip shear zones resulted in fast exhumation and SW-ward extrusion of the basement rocks and granite plutons of the Tengchong Terrane. This deformation geometry indicates the importance of mid-crustal detachments in accommodating the large displacements of continental fragments in a transpression orogen.

Supplementary data to this article can be found online at http://dx.doi.org/10.1016/j.tecto.2015.09.033.

Acknowledgments

We thank Profs. Arnaud Pêcher, Maurice Brunel and A. Alexander G. Webb for constructive discussion, and F.Y. Chen and M. Zhang for their assistances in the EBSD measurements and drawing figures. Suggestions from Prof. An Yin and one anonymous reviewer helped us to polish the manuscript carefully. This study was supported by the National Natural Science Foundation of China (No. 40921001) and the Geological Survey of China (No.1212010818094).

References

Akciz, S., Burchfiel, B.C., Crowley, J.L., Yin, J.Y., Chen, L.Z., 2008. Geometry, kinematics, and regional significance of the Chong Shan shear zone, Eastern Himalayan Syntaxis, Yunnan, China. Geosphere 4, 292–314.

Armijo, R., Tapponnier, P., Han, T.L., 1989. Late Cenozoic right-lateral strike-slip faulting in southern Tibet. J. Geophys. Res. 94, 2787–2838.

Barth, N.C., Hacker, B.R., Seward, G.G.E., Walsh, E.O., Young, D., Johnston, S., 2010. Strain within the ultrahigh-pressure Western Gneiss region of Norway recorded by quartz CPOs. In: Law, R.D., Butler, R.W. H., Holdsworth, R.E., Krabbendam, M., Strachan, R.A. (Eds.), Continental tectonics and mountain building: the legacy of Peach and Horne. Geological Society, London, Special Publications 335, pp. 663–685.

Beaumont, C., Jamieson, R.A., Nguyen, M.H., Lee, B., 2001. Himalayan tectonics explained by extrusion of a low-viscosity crustal channel coupled to focused surface denudation. Nature 414, 738–742. http://dx.doi.org/10.1038/414738A.

Bertrand, G., Rangin, C., Maluski, H., Han, T.A., Thien, M., Myint, O., Maw, W., Lwin, S., 1999. Cenozoic metamorphism along the Shan scarp (Myanmar): Evidence for ductile shear along the Sagaing fault or northward migration of the eastern Himalayan syntaxis? Geophys. Res. Lett. 26, 915–918.

Bertrand, G., Rangin, C., Maluski, H., Bellon, H., 2001. Diachronous cooling along the Mogok Metamorphic Belt (Shan scarp, Myanmar): The trace of the northward migration of the Indian syntaxis. J. Asian Earth Sci. 19, 649–659.

Blumenfeld, P., Mainprice, D., Bouches, J.L., 1986. C-slip in quartz from subsolidus deformed granite. Tectonophysics 127, 97–115.

Bonamici, C.E., Tikoff, B., Goodwin, L.B., 2011. Anatomy of a 10 km scale sheath fold, Mount Hay ridge, Arunta Region, central Australia: The structural record of deep crustal flow. Tectonics 30, TC6015. http://dx.doi.org/10.1029/2011TC002873.

Burchfiel, B.C., Chen, Z., 2012. Tectonics of the Southeastern Tibetan Plateau and its adjacent foreland. Geol. Soc. Am. Mem. 210 (231p.).

Bureau of Geology and Mineral Resources of Yunnan Province, 1990. Regional geology of Yunnan Province. Geological Publishing House, Beijing.

Cai, Z.H., Xu, Z.Q., Duan, X.D., Li, H.Q., Cao, H., Huang, X.M., 2013. Early stage of Early Paleozoic orogenic event in western Yunnan Province, southeastern margin of Tibet Plateau. Acta Petrol. Sin. 29, 2123–2140.

Chung, S.L., Lee, T.Y., Lo, C.H., Wang, P.L., Chen, C.Y., Yem, N.T., Hoa, T.T., Genyao, W., 1997. Intraplate extension prior to continental extrusion along the Ailaoshan-Red River shear zone. Geology 25, 311–314.

Chung, S.L., Chu, M.F., Zhang, Y.Q., Xie, Y.W., Lo, C.H., Lee, T., Lan, C.Y., Li, X.H., Zhang, Q., Wang, Y.Z., 2005. Tibetan tectonic evolution inferred from spatial and temporal variations in post-collisional magmatism. Earth Sci. Rev. 68, 173–196.

Claoué-Long, J.G., Compston, W., Roberts, J., Fanning, C.M., 1995. Two Carboniferous ages: A comparison of SHRIMP zircon dating with conventional zircon ages and $^{40}Ar/^{39}Ar$ analysis. In: Berggren, W.A., Kent, D.V., Aubry, M.-P., Hardenbol, J. (Eds.), Geochronology, time scale and global stratigraphic correlation. SEPM (Society for Sedimentary Geology) Special Publication 4, pp. 3–21.

Clark, M.K., Royden, L.H., 2000. Topographic ooze: Building the eastern margin of Tibet by lower crustal flow. Geology 28, 703–706.

Dong, F.L., Hou, Z.Q., Gao, Y.F., Zeng, P.S., Jiang, C.X., 2006. Cenozoic granitoid in Tengchong, western Yunnan: Genesis type and implication for tectonics. Acta Petrol. Sin. 22, 927–937.

Dumond, G., Goncalves, P., Williams, M.L., Jercinovic, M.J., 2010. Subhorizontal fabric in exhumed continental lower crust and implications for lower crustal flow: Athabasca granulite Terrane, western Canadian Shield. Tectonics 29, TC2006. http://dx.doi.org/10.1029/2009TC002514.

England, P., Houseman, G., 1986. Finite strain calculations of continental deformation 2. Comparison with the India-Asia collision zone. J. Geophys. Res. 91, 3664–3676.

Eskola, P.E., 1949. The problem of mantled gneiss domes. Geol. Soc. Lond. Q. J. 104, 461–476.

Gan, W., Zhang, P., Shen, Z.-K., Niu, Z., Wang, M., Wan, Y., Zhou, D., Cheng, J., 2007. Present-day crustal motion within the Tibetan Plateau inferred from GPS measurements. J. Geophys. Res. 112, B08416. http://dx.doi.org/10.1029/2005JB004120.

Gilley, L.D., Harrison, T.M., Leloup, P.H., Ryerson, F.J., Lovera, O.M., Wang, J.H., 2003. Direct dating of left-lateral deformation along the Red River shear zone, China and Vietnam. J. Geophys. Res. 103, 21–27.

Godin, L., Grujic, D., Law, R.D., Searle, M.P., 2006. Channel flow, ductile extrusion and exhumation in continental collision zones: an introduction. In: Law, R.D., Searle, M.P., Godin, L. (Eds.), Channel flow, ductile extrusion and exhumation in continental collision zones. Geological Society, London, Special Publications 268, pp. 1–23.

Grujic, D., 2006. Channel flow and continental collision tectonics: an overview. In: Law, R.D., Searle, M.P., Godin, L. (Eds.), Channel flow, ductile extrusion and exhumation in continental collision zones. Geological Society, London, Special Publications 268, pp. 25–37.

Harrison, T.M., 1981. Diffusion of ^{40}Ar in hornblende. Contrib. Mineral. Petrol. 78, 324–331.

Harrison, T.M., Duncan, I., McDougall, I., 1985. Diffusion of ^{40}Ar in biotite: temperature, pressure, and compositional effects. Geochim. Cosmochim. Acta 49, 2461–2468.

Harrison, T.M., Leloup, P.H., Ryerson, F.J., Tapponnier, P., Lacassin, R., Chen, W., 1996. Diachronous initiation of transtension along the Ailao Shan-Red River shear zone, Yunnan and Vietnam. In: Harrison, T.M. (Ed.), Yin, A. Cambridge University Press, The Tectonic Evolution of Asia, pp. 208–225.

Harrison, T.M., Célérier, J., Aikman, A.B., Hermann, J., Heizler, M.T., 2009. Diffusion of ^{40}Ar in muscovite. Geochim. Cosmochim. Acta 73, 1039–1051.

Hoskin, P.W.O., Schaltegge, U., 2003. The composition of zircon and igneous and metamorphic petrogenesis. In: Hanchar, J.M., Hoskin, P.W.O. (Eds.), Rev. Mineral. Geochem. 53. Mineralogical Society of America, Washington, D.C., pp. 27–62

Houseman, G., England, P., 1986. Finite strain calculations of continental deformation 1. Method and general results for convergent zones. J. Geophys. Res. 91, 3651–3663.

Ji, J.Q., Zhong, D.L., Sang, H.Q., Zhang, L.S., 2000. The western boundary of extrusion blocks in the southeastern Tibetan Plateau. Chin. Sci. Bull. 45, 870–875.

Jiang, B., Gong, Q.J., Zhang, J., Ma, N., 2012. Late Cretaceous aluminum A-type granites and its geological significance of Dasongpo Sn deposit, Tengchong, West Yunnan. Acta Petrol. Sin. 28, 1477–1492.

Jolivet, L., Beyssac, O., Goffe, B., Avigad, D., Lepvrier, C., Maluski, H., Thang, T.T., 2001. Oligo-Miocene midcrustal subhorizontal shear zone in Indochina. Tectonics 20, 46–57.

Kornfeld, D., Eckert, S., Appel, E., Ratschbacher, L., Sonntag, B.-L., Pfänder, J.A., Ding, L., Liu, D., 2014a. Cenozoic clockwise rotation of the Tengchong block, southeastern Tibetan Plateau: A paleomagnetic and geochronologic study. Tectonophysics 628, 105–122.

Kornfeld, D., Sonntag, B.-L., Matthes, J., Ratschbacher, L., Pfänder, J.A., Eckert, S., Liu, D., Appel, E., Ding, L., 2014b. Apparent paleomagnetic rotations reveal Pliocene–Holocene internal deformation of the Tengchong Block, southeastern Tibetan Plateau. J. Asian Earth Sci. 96, 1–16.
Lee, H.Y., Chung, S.L., Wang, J.R., Wen, D.J., Lo, C.H., Yang, T.F., Zhang, Y.Q., Xie, Y.W., Lee, T.Y., Wu, G.Y., Ji, J.Q., 2003. Miocene Jiali faulting and its implications for Tibetan tectonic evolution. Earth Planet. Sci. Lett. 205, 185–194.
Leloup, P.H., Lasassin, R., Tapponnier, P., Zhong, D., Liu, X., Zhang, L., Ji, S., Trinh, P.T., 1995. The Ailao Shan-Red River shear zone (Yunnan, China), Tertiary transform boundary of Indochina. Tectonophysics 251, 3–84.
Leloup, P.H., Arnaud, N., Lacassin, R., Kienast, J.R., Harrison, T.M., Phan Trong, T.T., Replumaz, A., Tapponnier, P., 2001. New constraints on the structure, thermochronology, and timing of the Ailao Shan-Red River shear zone, SE Asia. J. Geophys. Res. 106, 6683–6732.
Li, D.M., Li, Q., Chen, W.J., 2000. Volcanic activities in the Tengchong volcano area since Pliocene. Acta Petrol. Sin. 16, 362–370.
Lin, T.H., Lo, C.H., Chung, S.L., Hsu, F.J., Yeh, M.W., Lee, T.Y., Ji, J.Q., Wang, Y.Z., Liu, D.Y., 2009. $^{40}Ar/^{39}Ar$ dating of the Jiali and Gaoligong shear zones: Implications for crustal deformation around the Eastern Himalayan Syntaxis. J. Asian Earth Sci. 34, 674–685.
Lin, S.L., Cong, F., Gao, Y.J., Zou, G.F., 2012. LA-ICP-MS zircon U-Pb age of gneiss from Gaoligong Mountain Group on the southeastern margin of Tengchong block in western Yunnan Province. Geol. Bull. China 31, 258–263.
Liu, J.L., Cao, S.Y., Zhang, Y.F., et al., 2007. Rotation of crustal blocks as an explanation of Oligo-Miocene extension in southeastern Tibet – evidenced by the Dancangshan and nearby metamorphic core complexes. Earth Sci. Front. 14, 40–48.
Liu, F.L., Wang, F., Liu, P.H., Yang, H., Meng, E., 2015. Multiple partial melting in the Ailaoshan-Red River and Gaoligong Shan complex belts, SE Tibetan Plateau: Zircon U-Pb dating of granitic leucosomes within migmatites. J. Asian Earth Sci. 110, 151–169.
Ma, N., Deng, J., Wang, Q.F., Wang, C.M., Zhang, J., Li, G.J., 2013. Geochronology of the Dasongpo tin deposit, Yunnan Province: Evidence from zircon LA-ICP-MS U-Pb age. Acta Petrol. Sin. 29, 1223–1235.
Ma, L.Y., Wang, Y.J., Fan, W.M., Geng, H.Y., Cai, Y.F., Zhong, H., Liu, H.C., Xing, X.W., 2014. Petrogenesis of the early Eocene I-type granites in west Yingjiang (SW Yunnan) and its implication for the eastern extension of the Gangdese batholiths. Gondwana Res. 25, 401–419.
Mainprice, D., 1990. A Fortran program to calculate seismic anisotropy from the lattice preferred orientation of minerals. Comput. Geosci. 16, 385–393.
Mainprice, D., Bouchez, J.L., Blumenfeld, P., Tubià, J.M., 1986. Dominant c slip in naturally deformed quartz: Implications for dramatic plastic softening at high temperature. Geology 14, 819–822.
Metcalfe, I., 2006. Palaeozoic and Mesozoic tectonic evolution and palaeogeography of East Asian crustal fragments: The Korean Peninsula in context. Gondwana Res. 9, 24–46.
Mitchell, A.H.G., 1993. Cretaceous-Cenozoic tectonic events in western Myanmar (Burma)-Assam region. J. Geol. Soc. Lond. 150, 1089–1102.
Mitchell, A.H.G., Chung, S.-L., Oo, T., Lin, T.-H., Huang, C.-H., 2012. Zircon U-Pb ages in Myanmar: Magmatic-metamorphic events and the closure of a Neo-Tethys ocean? J. Asian Earth Sci. 56, 1–23.
Molnar, P., Stock, J.M., 2009. Slowing of India's convergence with Eurasia since 20 Ma and its implications for Tibetan mantle dynamics. Tectonics 28, TC3001. http://dx.doi.org/10.1029/2008TC002271.
Najman, Y., et al., 2010. Timing of India-Asia collision: Geological, biostratigraphic, and palaeomagnetic constraints. J. Geophys. Res. 115, B12416. http://dx.doi.org/10.1029/2010JB007673.
Otofuji, Y., Yokoyama, M., Kitada, K., Zaman, H., 2010. Paleomagnetic versus GPS determined tectonic rotation around eastern Himalayan syntaxis in East Asia. J. Asian Earth Sci. 37, 438–451.
Parrish, R.R., 2001. The response of mineral chronometers to metamorphism and deformation in orogenic belts. In: Miller, J.A., Holdsworth, R.E., Buick, I.S., Hand, M. (Eds.), Continental reactivation and reworking. The Geological Society of London, pp. 289–301.
Passchier, C.W., Trouw, R.A.J., 2005. Microtectonics. Springer, Germany, p. 366.
Peltzer, G., Tapponnier, P., 1988. Formation and evolution of strike-slip faults, rifts and basins during the India-Asia collision – An experimental approach. J. Geophys. Res. 93, 15085–15117.
Qi, X., Zhu, L., Grimmer, J.C., Hu, Z., 2015. Tracing the Transhimalayan magmatic belt and the Lhasa block southward using zircon U–Pb, Lu–Hf isotopic and geochemical data: Cretaceous-Cenozoic granitoids in the Tengchong block, Yunnan, China. J. Asian Earth Sci. 110, 170–188.
Ratschbacher, L., Frisch, W., Chen, C., Pan, G., 1996. Cenozoic deformation, rotation, and stress patterns in eastern Tibet and western Sichuan, China. In: Yin, A., Harrison, T.M. (Eds.), The tectonic evolution of Asia. Cambridge University Press, Cambridge, pp. 227–249.
Replumaz, A., Tapponnier, P., 2003. Reconstruction of the deformed collision zone Between India and Asia by backward motion of lithospheric blocks. J. Geophys. Res. 108, 2285. http://dx.doi.org/10.1029/2001JB000661.
Royden, L.H., Burchfiel, B.C., van der Hilst, R.D., 2008. The geological evolution of the Tibetan Plateau. Science 321, 1054–1058.
Schmid, S.M., Casey, M., 1986. Complete fabric analysis of some commonly observed quartz c-axis patterns. Mineral and Rock Deformation: Laboratory studies, The Paterson VolumeHobbs, B.E., Heard, H.C. 36. American Geophysical Union, Washington DC, pp. 263–286.
Searle, M.P., Noble, S.R., Cottle, J.M., Waters, D.J., Mitchell, A.H.G., Hlaing, T., Horstwood, M.S.A., 2007. Tectonic evolution of the Mogok metamorphic belt, Burma (Myanmar) constrained by U-Th-Pb dating of metamorphic and magmatic rocks. Tectonics 26, 1–24.
Shen, Z.-K., Lü, J., Wang, M., Bürgmann, R., 2005. Contemporary crustal deformation around the southeast borderland of the Tibetan Plateau. J. Geophys. Res. 110, B11409. http://dx.doi.org/10.1029/2004JB003421.
Socquet, A., Pubellier, M., 2005. Cenozoic deformation in western Yunnan (China-Myanmar border). J. Asian Earth Sci. 24, 495–515.
Stipp, M., Stünitz, H., Heilbronner, R., Schimid, S.M., 2002. The eastern Tonale fault zone: A "natural laboratory" for crystal plastic deformation of quartz over a temperature range from 250 to 700 °C. J. Struct. Geol. 24, 1861–1884.
Tapponnier, P., Molnar, P., 1976. Slip line field theory and large scale continental tectonics. Nature 264, 319–324.
Tapponnier, P., Peltzer, G., Armijo, R., 1986. On the mechanics of the collision between India and Asia. In: Coward, M.P., Ries, A.C. (Eds.), Collision tectonics. Geological Society London Special Publications 19, pp. 115–157.
Tapponnier, P., Xu, Z.Q., Roger, F., Meyer, B., Arnaud, N., Wittlinger, G., Yang, J.S., 2001. Oblique stepwise rise and growth of the Tibet Plateau. Science 294, 1671–1677.
Thatcher, W., 2007. Microplate model for the present-day deformation of Tibet. J. Geophys. Res. 112, B01401. http://dx.doi.org/10.1029/2005JB004244.
Vanderhaeghe, O., Teyssier, C., Wysoczanski, R., 1999. Structural and geochronological constraints on the role of partial melting during the formation of the Shuswap metamorphic core complex at the latitude of the Thor–Odin dome, British Columbia. Can. J. Earth Sci. 36, 917–943.
Wang, E.C., Burchfiel, B.C., 1997. Interpretation of Cenozoic tectonics in the right lateral accommodation zone between the Ailao Shan Shear Zone and the Eastern Himalayan Syntaxis. Int. Geol. Rev. 39, 191–219.
Wang, E.C., Burchfiel, B.C., Royden, L.H., Chen, L.Z., Chen, J.S., Li, W.X., Chen, Z.L., 1998. The late Cenozoic Xianshuihe–Xiaojiang, Red River, and Dali fault systems of southwestern Sichuan and central Yunnan, China. Geol. Soc. Am. Spec. Pap. 327 (108 p).
Wang, Y.J., Fan, W.M., Zhang, Y.H., Peng, T.P., Chen, X.Y., Xu, Y.G., 2006. Kinematics and $^{40}Ar/^{39}Ar$ geochronology of the Gaoligong and Chongshan shear systems, western Yunnan, China: implications for early Oligocene tectonic extrusion of SE Asia. Tectonophysics 418, 235–254.
Wang, G., Wan, J.L., Wang, E.C., Zheng, D.W., Li, F., 2008. Late Cenozoic to recent transtensional deformation across the Southern part of the Gaoligong shear zone between the Indian plate and SE margin of the Tibetan plateau and its tectonic origin. Tectonophysics 460, 1–20.
Watson, E.B., Wark, D.A., Thomos, J.B., 2006. Crystallization thermometers for zircon and rutile. Contrib. Mineral. Petrol. 151, 413–433.
Whitney, D.L., Teyssier, C., Vanderhaeghe, O., 2004. Gneiss domes and crustal flow. In: Whitney, D.L., Teyssier, C., Siddoway, C.S. (Eds.), Gneiss domes in orogeny. Geological Society of America Special Paper 380, pp. 15–33.
Williams, I.S., 1998. U–Th–Pb geochronology by ion microprobe. In: McKibben, M.A., Shanks III, W.C., Ridley, W.I. (Eds.), Applications of microanalytical techniques to understanding mineralizing processes. Rev. Econ. Geol., pp. 1–35.
Xu, Z.Q., Wang, Q., Tang, Z.M., Chen, F.Y., 2009. Fabric kinematics of ultrahigh-pressure metamorphic rocks from the main borehole of the Chinese Continental Scientific Drilling Project: Implications for continental subduction and exhumation. Tectonophysics 475, 235–250.
Xu, Y.G., Yang, Q.J., Lan, J.B., Luo, Z.Y., Huang, X.L., Shi, Y.R., Xie, L.W., 2012. Temporal-spatial distribution and tectonic implications of the batholiths in the Gaoligong–Tengliang–Yingjiang area, western Yunnan: constraints from zircon U–Pb ages and Hf isotopes. J. Asian Earth Sci. 53, 151–175.
Yang, Q.J., Xu, Y.G., Huang, X.L., Luo, Z.Y., Shi, Y.R., 2009. Geochronology and geochemistry of granites in the Tengchong area, western Yunnan: Tectonic implication. Acta Petrol. Sin. 25, 1092–1104.
Yin, A., 2004. Gneiss domes and gneiss dome systems. In: Whitney, D.L., Teyssier, C., Siddoway, C.S. (Eds.), Gneiss domes in orogenyGeological Society of America Special Paper 380. Boulder, Colorado, pp. 1–14.
Yin, A., 2006. Cenozoic tectonic evolution of the Himalayan orogen as constrained by along-strike variation of structural geometry, exhumation history, and foreland sedimentation. Earth Sci. Rev. 76, 1–131.
Yin, A., 2010. Cenozoic tectonic evolution of Asia: A preliminary synthesis. Tectonophysics 488, 293–325.
Zhang, P.Z., Shen, Z., Wang, M., Gan, W.J., Burgmann, R., Molnar, P., 2004. Continuous deformation of the Tibetan Plateau from global positioning system data. Geology 32, 809–812.
Zhang, B., Zhang, J.J., Zhong, D.L., Yang, L.K., Yue, Y.H., Yan, S.Y., 2012. Polystage deformation of the Gaoligong metamorphic zone: Structures, $^{40}Ar/^{39}Ar$ mica ages, and tectonic implications. J. Struct. Geol. 37, 1–18.
Zhong, D.L., 1998. Paleotethyan orogenic belts in Yunnan and western Sichuan. Science Press, Beijing.
Zhou, S., Mo, X.X., Dong, G.C., Zhao, Z.D., Qiu, R.Z., Guo, T.Y., Wang, L.L., 2004. $^{40}Ar–^{39}Ar$ geochronology of Cenozoic Linzizong volcanic rocks from Linzhou Basin, Tibet, China, and their geological implications. China Sci. Bull. 49, 1970–1979.
Zhu, D.C., Mo, X.X., Niu, Y.L., Zhao, Z.D., Wang, L.Q., Liu, Y.S., Wu, F.Y., 2009a. Geochemical investigation of Early Cretaceous igneous rocks along an east–west traverse throughout the central Lhasa Terrane, Tibet. Chem. Geol. 268, 298–312.
Zhu, M.Z., Graham, S., McHargue, T., 2009b. The Red River Fault zone in the Yinggehai Basin, South China Sea. Tectonophysics 476, 397–417.
Zhu, D.C., Zhao, Z.D., Niu, Y.L., Mo, X.X., Chung, S.L., Hou, Z.Q., Wang, L.Q., Wu, F.Y., 2011. The Lhasa Terrane: Record of a microcontinent and its histories of drift and growth. Earth Planet. Sci. Lett. 301, 241–255.
Zhu, R.Z., Lai, S.C., Qin, J.F., Zhao, S.W., 2015. Early-Cretaceous highly fractionated I-type granites from the northern Tengchong block, western Yunnan, SW China: Petrogenesis and tectonic implications. J. Asian Earth Sci. 100, 145–163.